DOCTORAL DISSERTATION

博士論文

CONSTITUTIVE MODEL CONSIDERING DENSITY EFFECT FOR CRUSHABLE SOILS AND ITS APPLICATION FOR GEOTECHNICAL PROBLEMS

密度の影響を考慮した破砕性土の構成モデルとその地盤
工学的問題への応用

Yokohama National University

Graduate School of Urban Innovation

国立大学法人横浜国立大学大学院都市イノベーション学府

NGUYEN TRONG NGHIA

グウェン　トロン　ギア

September 2022

2022 年 9 月

CONSTITUTIVE MODEL CONSIDERING DENSITY EFFECT FOR CRUSHABLE SOILS AND ITS APPLICATION FOR GEOTECHNICAL PROBLEMS

密度の影響を考慮した破砕性土の構成モデルとその地盤工学的問題への応用

by

NGUYEN TRONG NGHIA

グウェン　トロン　ギア

A Dissertation Submitted to the Graduate School of Urban Innovation, Yokohama National University in Partial Fulfillment of the Requirement for the Degree of

Doctor of Engineering

Yokohama National University, Graduate School of Urban Innovation

国立大学法人横浜国立大学大学院都市イノベーション学府

<u>Examination Committee</u>
Professor, Dr. Mamoru KIKUMOTO (Chair)

Professor, Dr. Kimitoshi HAYANO

Associate Professor, Dr. Ying CUI

Professor, Dr. Koichi MAIKAWA

Associate Professor, Dr. Hiroshi TAMURA

September 2022

2022 年 9 月

ABSTRACT

Ground exhibiting particle crushing can strongly affect foundation structures especially pile foundations with large magnitude of stresses at the pile's tip. In order to obtain a rational estimation of deformation and failure, numerical simulation with an appropriate constitutive model of crushable soils is necessary. Thus, the aims of this study are: 1) to establish a rational constitutive model of crushable soils which incorporates the effect of packing density; 2) to conduct numerical simulations with implementation of the proposed model for pile foundation problems.

The first section of this study is concerned with the constitutive model of crushable soils, which is based on a novel evolution law for grading index and incorporates the effect of packing density on particle crushing phenomena via the coordination number as an intermediate variable. The proposed constitutive model's validity was confirmed by comparing simulation results to a comprehensive set of elementary tests. The proposed model's advantage is its ability to predict seemingly contradictory experimental evidence for crushable soil: Under the same effective stress path, densely packed soil crushes less than loosely packed soil; densely packed soil crushes more than loosely packed soil when sheared under drained or undrained conditions. The non-uniqueness of the critical lines under the effect of density are also revealed due to the variations of peak strength with confining pressure.

The second section of this research focuses on numerical simulations of single pile foundations on crushable soils. The proposed model incorporates User-Defined-Material (USDM) simulations using FEM (by PLAXIS). Preliminary simulation results show that the breakage zone around the pile's tip and pile shaft is consistent with previous experimental studies. Based on the distribution of deviator strain, the failure mode of single pile may be the punching shear mode. In the load-settlement curves, densely packed soil exhibits more breakage and higher load than loosely packed soil. In the simulation with different densities, similar stress paths are detected for both simulations with loose and dense soils. However, the magnitudes of deviator stress and mean effective stress are higher for the simulation with dense soil. Therefore, more crushing is detected for the elements under pile tips of dense soil as compared to the loose soil. Also, more crushing occurs for the element locates on the assumed shear band than the element outside due to higher deviator stress. At the elements under pile's type, higher breakage is reported for loose soil at the same mean effective stress as compared to that of the dense soil.

ACKNOWLEDGEMENTS

TABLE OF CONTENTS

LIST OF FIGURES

LIST OF TABLES

Chapter 1 : Introduction

1.1 Research background

Soil particles can be crushed into smaller particles under high pressure, leading the large contraction and deformation. Thus, crushable soils cause significant issues to constructions or existing (Angemeer, Carlson et al. 1975, Dutt and Cheng 1984, Poulos and Chua 1985, Ismael and Al‐Sanad 1986, Murff 1987, Senders, Banimahd et al. 2013, White, Boylan et al. 2013). Due to wide distributions of crushable soils around the world (Carbonate sands in the coral reef regions, volcanic soils in the volcanic activity zones, and decomposed granite in the heavily weathering zones), studies of the behavior of these crushable soils have been extensively carried out: Coop (1990), conducted low and high pressure triaxial tests on a calcareous sand to examine the mechanical properties; Lee and Farhoomand (1967), performed anisotropic triaxial compression to create a similar stress state under the earth dam to observe behavior of particle crushing; Bandini and Coop (2011), studied the effect of particle crushing on the location of the critical state line of sands. Especially, several studies examined the effect of packing density on the breakage responses of crushable soils (Valdes 2003, Guimaraes, Valdes et al. 2007, Altuhafi and Coop 2011, Shahnazari and Rezvani 2013, Hyodo, Wu et al. 2017). In the studies, densely packed soil exhibits lesser crushing than loosely packed soil under the same effective stress path. On the other hand, densely packed soil is more likely to crush than loosely packed one when it is sheared under drained or undrained conditions. Thus, the state of density of the crushable soils can control the breakage responses.

Large magnitude of stress at the tip of pile foundation can cause particle crushing and effect pile's behavior (Yasufuku and Hyde 1995, Kuwajima, Hyodo et al. 2009). The region adjacent to the pile shaft also subjected to high shear stress which leaded to particle crushing. There was also a report of the reduction pile resistances when they rested on the calcareous soils in the western coast of Australia (Senders, Banimahd et al. 2013). Thus, the pile's responses are very sensitive with the ground exhibiting particle crushing. In an attempt to determine the responses of piles on crushable soils, several numerical simulations of pile penetration on crushable soils were performed. Zhang, Nguyen et al.

(2013), simulated pile penetration on the crushable soil by incorporating a constitutive model based on the framework of thermodynamic. Jin, Yin et al. (2018) performed numerical simulation of pile penetration with a constitutive model based on the framework of multi-surface plasticity accounting for the effects of stress dilatancy and particle crushing. However, their constitutive models did not consider the effect of density on the breakage responses. Thus, the simulations can only be applied for a certain packing density.

1.1.1 Effect of density on the breakage responses

In this section, fundamental responses of the crushable soil with the effect of packing density under different stress path are illustrated through experimental evidence. Confirming by many studies (Valdes 2003, Guimaraes, Valdes et al. 2007, Altuhafi and Coop 2011, Shahnazari and Rezvani 2013, Hyodo, Wu et al. 2017), under consolidation tests (the same tress path), the densely packed soils exhibited less particle crushing. Altuhafi and Coop (2011), performed 1D consolidation tests with three different initial densities ($e_o = 1.486$, $e_o = 1.672$, and $e_o = 1.863$) for Dogs Bay sand up to very high compression pressure of 30 MPa. Figs. (1-1a) and (1-1b) shows the compression curves of these tests and particle size distributions (PSD) after the tests, respectively. In these figures, the PSD of the denser soils showed less broaden than the looser soils indicating that less breakage occurred for the denser soils. The similar trend was also observed in isotropic consolidation tests conducted by Hyodo, Wu et al. (2017) for Aio sand; 1D compression tests performed by Guimaraes, Valdes et al. (2007), (Shahnazari and Rezvani 2013) for Ottawa sand and Hormuz Island (HI) sand, respectively.

A remarkable breakage variation with the compressive stresses was presented under 1D consolidation tests of Ottawa sand by (Valdes 2003, Guimaraes, Valdes et al. 2007). Figure (1-2a) shows the compression curves and Figs. (1-2b), (1-2c) and (1-2d) illustrated the PSD for dense ($e_o = 0.534$) and loose ($e_o = 0.698$) soils at three desired compression pressures of 1.4 MPa, 50 MPa and 100 MPa. As can be observed in the Figs (1-2b), (1-2 c) and (1-2 d), PSD variations revealed that the breakage of the loose and dense soils varied when the compression pressure was increased. Generally,

the densely packed soil exhibited less crushing than the loosely packed soil and the variations reduced when the confining stress increased.
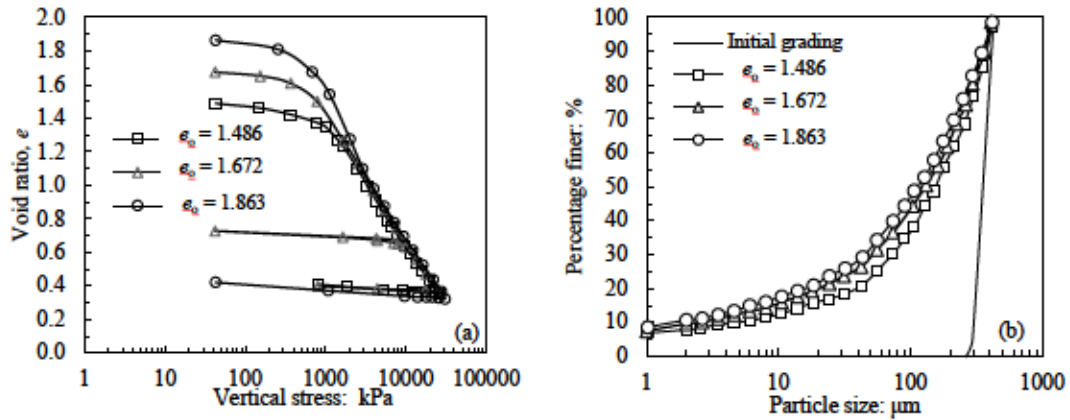
Figure 1-1: *1D consolidation for Dogs Bay sand: (a) compression curves in* $e - \log p'$; *(b) sieve analyses after test (after Altuhafi and Coop (2011)).*
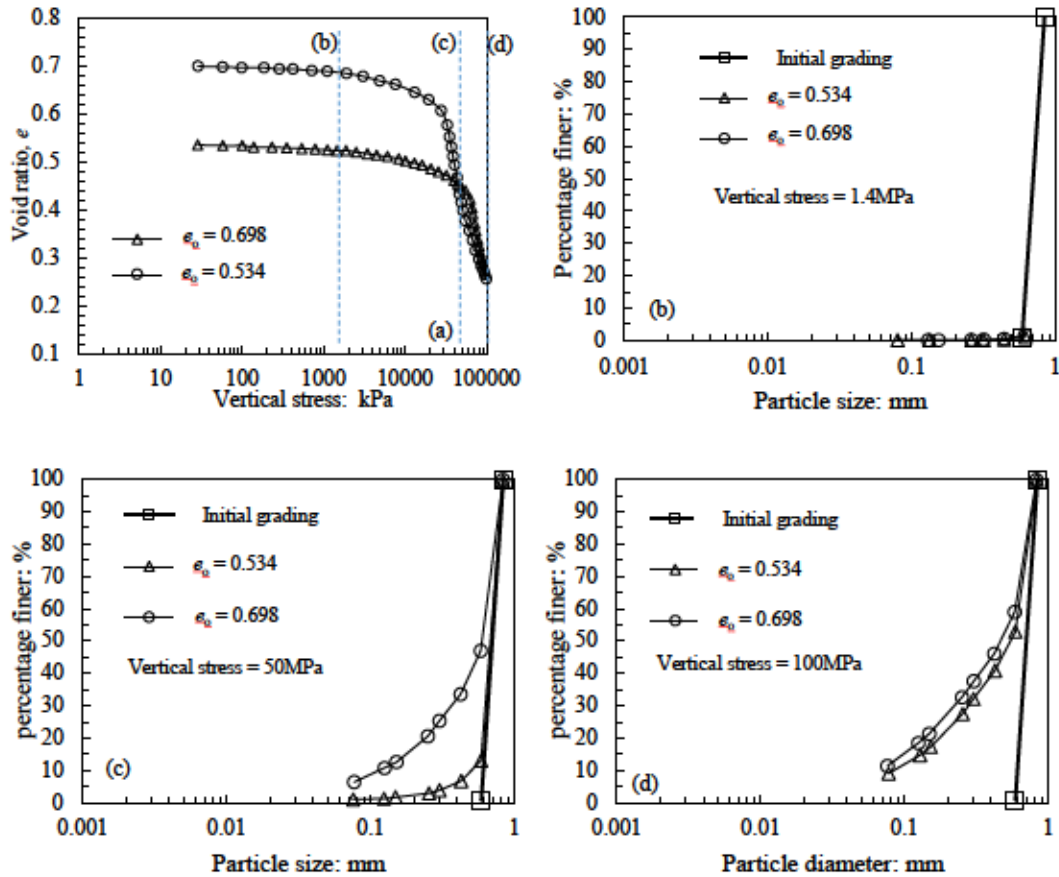
Figure 1-2: 1D consolidation test for Ottawa sand: (a) compression curves in $e-\log p'$; (b)-(d) PSDs at vertical stress of 1.4 MPa, 50MPa, 100 MPa, respectively (Valdes 2003, Guimaraes, Valdes et al. 2007).

On the other hand, a seemingly contradictory experimental evidence was observed in consolidated drained (CD) triaxial tests with constant radial stress and undrained triaxial tests (CU) by (Shahnazari and Rezvani 2013, Hyodo, Wu et al. 2017). This experimental evidence demonstrated that the densely packed soil exhibited more crushing than the loosely packed soils after the shearing state. Figs. (1-3a) and (1-3b) represent the shear deformation and variation of grading index, I_G , (an indicator of breakage, derived from the variations of relative breakage, B_r , (Hyodo, Wu et al. 2017) of the CU test carried out by Hyodo, Wu et al. (2017). After the shearing state (Fig. 1-3b), the higher value of grading index was detected for the denser soil ($e_0 = 0.657$) as compared to the looser soil ($e_0 = 0.760$) indicating that more breakage occurred in the denser soil as compared to the looser soil. Also, at the failure state (Fig. 1-3a), the stress of the denser soil was higher than that of the looser soil. These trends (higher stress and breakage for denser soil after the shearing state) were also confirmed in CD tests conducted for Hormuz Island (HI) sand by Shahnazari and Rezvani (2013) (Fig. 1-4) .
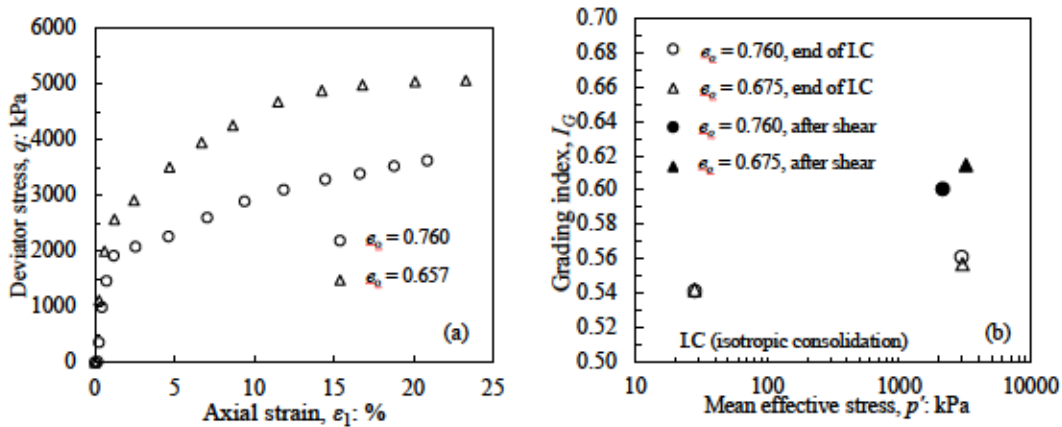
Figure 1-3: CU test for Aio sand: (a) deviator stresses versus axial strain; (b) variations of grading index (derived from relative breakage , B_r , Hyodo, Wu et al. (2017)) (after Hyodo, Wu et al. (2017)).
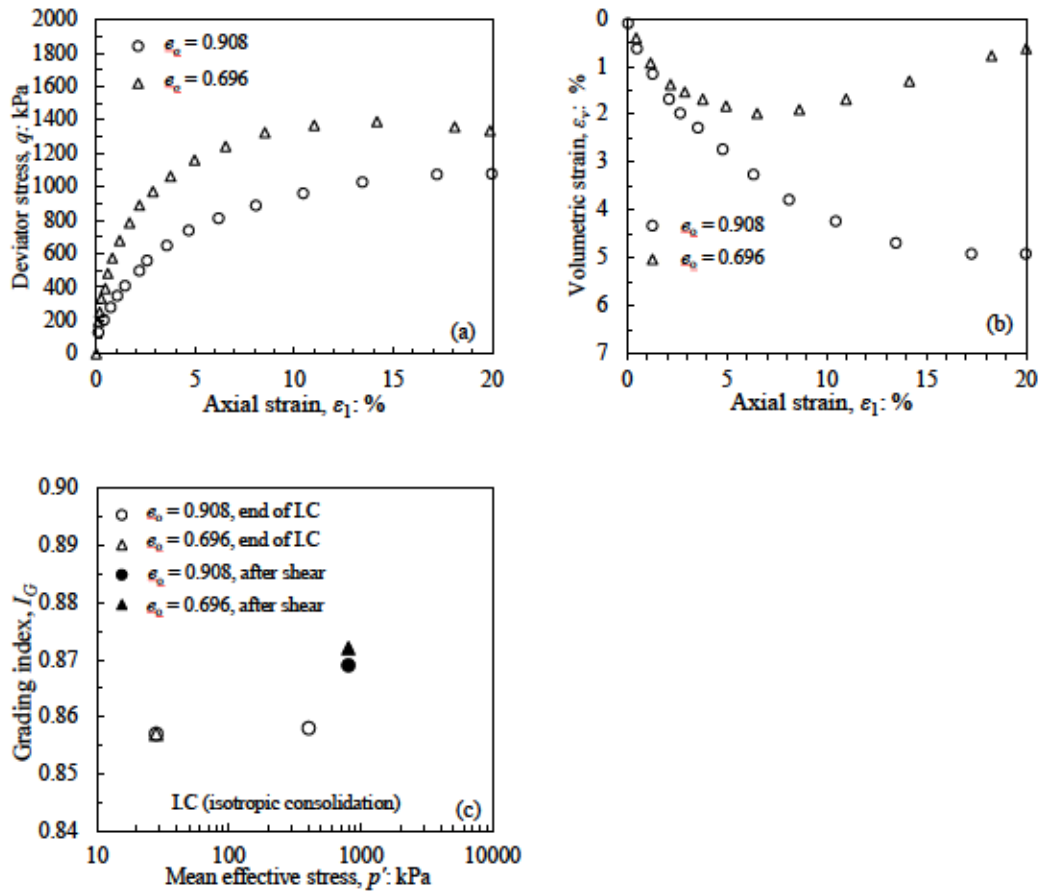
Figure 1-4: CD test with constant radial stress for HI sand and experimental results by Shahnazari and Rezvani (2013): (a) stress-strain responses; (b) volumetric responses; (b) variation of grading index with mean effective stress (derived from relative breakage, B_r, Shahnazari and Rezvani (2013)).

1.1.2 Mean coordination number and density

In microscopic view, the difference between each packing density is the different contact points or coordination numbers. In the context, the densely packed soils have higher coordination number as compared to the loosely packed soil. It is essential to examine the relationship between coordination number and density in order to correctly describe the crushing phenomena in section 1.1.1. The studied of Graton and Fraser (1935) for six typical systematic packings shown that the denser packing will lead to higher coordination number (Fig. 1-5). The similar trend also found in the studied of Aïm and le Goff (1968) (table 1-1). Subsequently, this was also confirmed experimental results of glass beads by Oda (1977); X-ray CT of Toyoura sand and glass beads by Matsushima, Uesugi et al. (2008); rounded stones

by Field (1963). Although there are extensive researchers and various of functions describing the relationship between the coordination number and density (German 2014). The relationship functions based on their own testing results therefore could not apply for a general case. Thus, it is needed to establish a general relationship function between mean coordination number and density.

Cubic
$C_N = 6; e_o = 0.91$

Orthorhombic
$C_N = 8; e_o = 0.47$

Rhombohedral
$C_N = 12; e_o = 0.35$

Orthorhombic
$C_N = 8; e_o = 0.47$

Tetragonal-Sphenoidal
$C_N = 10; e_o = 0.432$

Rhombohedral
$C_N = 12; e_o = 0.35$

C_N : the coordination number
e_o : the void ratio
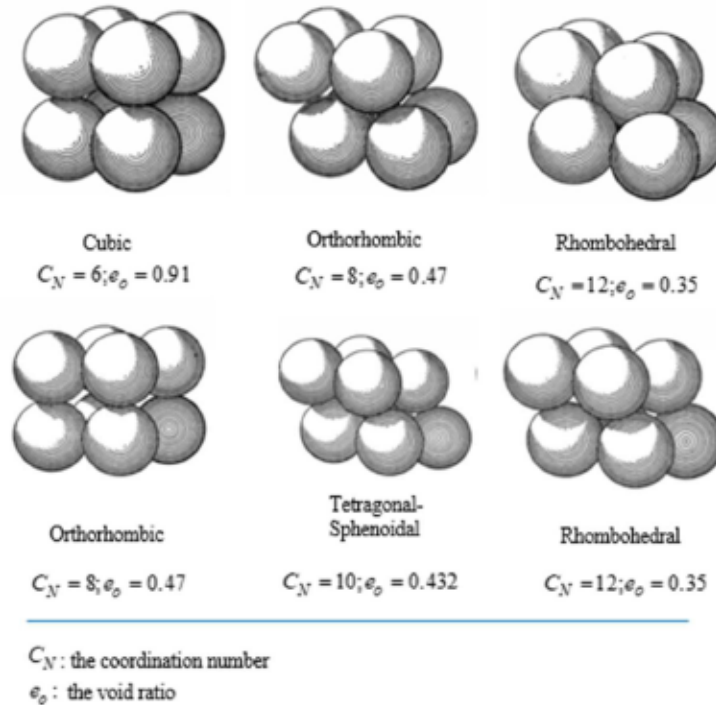
Figure 1-5: Systematic packing of six-typical packings (after Graton and Fraser (1935))

Table 1-1. Systematic packing (after Aïm and le Goff (1968))

Packing type	Coordination number, C_N	Void ratio, e_o
Hexagonal compact	12	0.35
Face-centered cubic	12	0.35
Rhombohedral	10	0.432
Centered cubic	8	0.47
Hexagonal	8	0.654
Simple cubic	6	0.91

1.1.3 Grading index and former evolution rules

The grading index is a fundamental factor for simply describing the crushing state of crushable soil. As particle crushing occurs, PSD evolves from a uniform grain size to the current grain size. The grading index, I_G, proposed by Muir Wood (2007) and Kikumoto, Wood et al. (2010) is used to describe the variation of PSD is illustrated in Fig. (1-6). As observed in Fig. (1-6), when crushing happens, grading index, I_G, varies from uniform grading with $I_G = 0$ to the limit grading with $I_G = 1$. Similarly, other researchers also considered a crushing index as potential breakage (Hardin 1985) or relative breakage (Einav 2007) to quantify the evolution of PSD. However, the advantage of the grading index, I_G, proposed by Muir Wood (2007) is that the evolution of grading is portrayed as a whole process (started from uniform grading to the limit grading) regardless of initial grading state. While, the breakage index proposed by Einav (2007) or Hardin (1985) considered initial grading as a starting point of breakage responses.
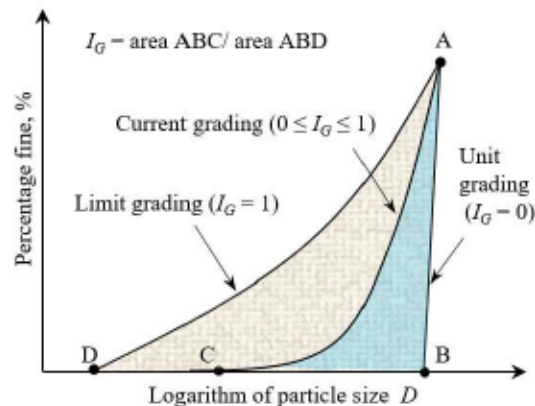
Figure 1-6: Definition of grading index (Muir Wood 2007)

The breakage responses can be depicted by the variations of these grading (Hardin 1985, Einav 2007, Muir Wood 2007, Kikumoto, Wood et al. 2010) through relationship with stress state or energy dissipation. The potential breakage, B_r, proposed by (Hardin 1985) could be expressed in the term of breakage effective stress through a hyperpolic equation. The relative breakage proposed by (Einav 2007) was considered as an interal variable in thermomechanical analysis. Grading index can be

expressed with the crushing stress crushing stress, p_x, (a composition of mean effective stress, p', and deviator stress, q) (Kikumoto, Wood et al. 2010):

$$I_G = 1 - \exp\left\{-\left(\frac{p_x - p_{xo}}{p_r}\right)^n\right\}$$ (1-1)

Where p_{xo} is the initial crushing stress, a stress point when particles start to crush. p_r is the crushing stress resistance which depends on the strength of particle. The higher value of p_r is, the more resistance of soils is against crushing. n is a parameter controlling the crushing stress ratio. None of these above evolution rule of crushing index considered the effect of packing density. Thus, the crushing responses under different densities might not capture properly by the constitutive model based on these evolution rules.

1.1.4 Pile foundation on crushable soils

The pile foundation is the most sensitive structure for crushable soils due to large stresses concentrated at the pile's tip and high shear stress along the pile's shaft. The particle crushing many caused reductions in pile's resistance. An in-situ pile foundation rested on the calcareous soils was reported with reduction of pile resistances (Senders, Banimahd et al. 2013). Experimental results by Kuwajima, Hyodo et al. (2009) and Yasufuku and Hyde (1995) also confirmed that the crushable soils showed less resistance as compared to the strong grain soil (Fig. 1-7). The compressed zone at pile's tip and shear zone adjacent pile's shaft illustrated in Fig. 1-8 showed that these regions were sensitive to particle crushing. Fig. 1-9 confirmed the particle crushing around pile's shaft through a study of cone penetration in sand by Arshad, Tehrani et al. (2014). Thus, pile resistance is reduced when pile rested on the crushable soils due to large among of crushed particles at the pile's tip and pile shaft.

Regarding the effect of densities on the responses of pile, experimental studies of pile penetration on Dogs Bay sand with different densities were performed by Yasufuku and Hyde (1995) (Fig. 1-10). As can be observed in Fig. 1-10, The ultimate bearing capacity could not be detected because the applied stress was still increased even a large the settlement ratio $S/D = 1.0$. The figure also shows that the higher relative density was, the higher applied stress was required for the same settlement.
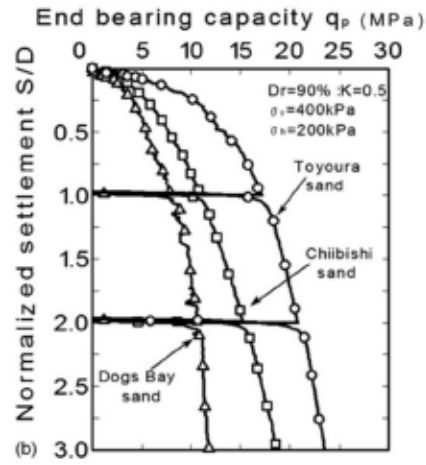
Figure 1-7: End bearing capacity for pile penetration tests (Kuwajima, Hyodo et al. 2009)

Dog Bays sand

Chibishi sand
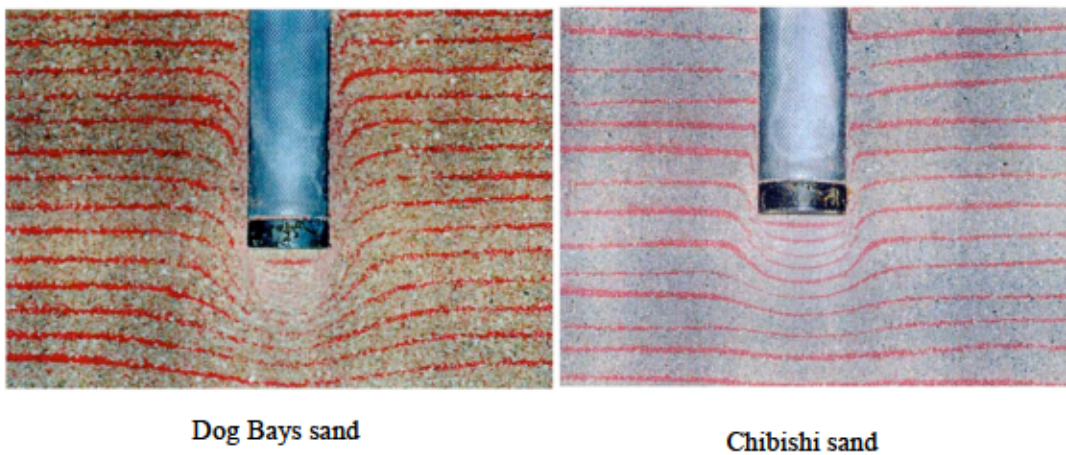
Figure 1-8: Compressed zone around pile's tipe and shear zone at pile's shaft (Kuwajima, Hyodo et al. 2009)
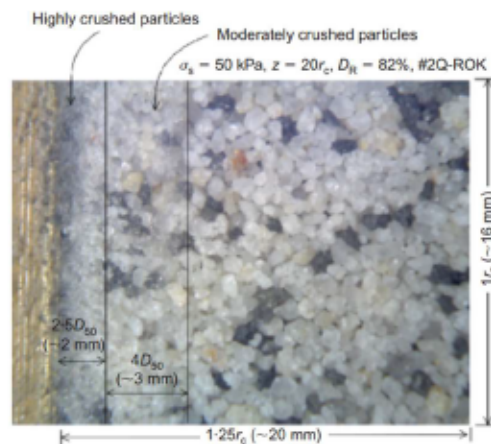
Figure 1-9: particle crushing around the pile's shaft (Arshad, Tehrani et al. 2014)
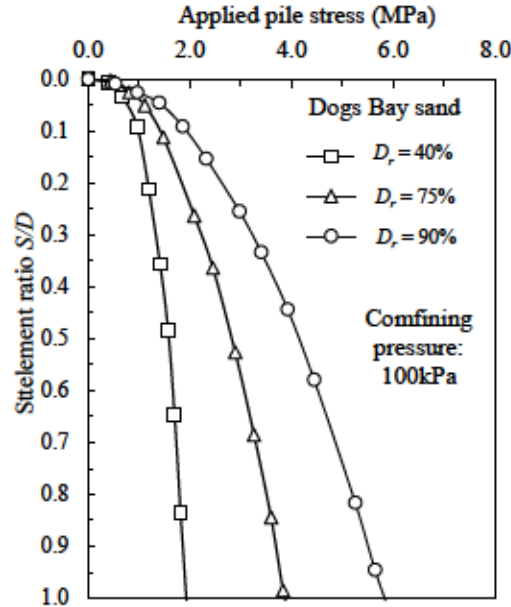
Figure 1-10: Pile load-settlement curves on Bogs Bay sand (after Yasufuku and Hyde (1995))

In order to capture the response of piles on the crushable soils, numerical simulations incorporating particle crushing were performed such as: Zhang, Nguyen et al. (2013) simulated pile penetration by incorporating a constitutive model based on the framework of thermodynamic; Jin, Yin et al. (2018) performed numerical simulation of pile penetration with a constitutive model based on the framework of multi-surface plasticity accounting for the effects of stress dilatancy and particle crushing. The simulations omitted the effect of density on pile responses. Furthermore, their constitutive model did not take account for the effect of density. Thus, it is necessary to establish a rational constitutive model for crushable soil and incorporate the proposed model to numerical simulations to examine the effect of packing density on the response on pile.

1.1.5 FEM outline

As mentioned earlier, the numerical simulation is necessary for pile foundation on crushable soils. In other to simplify modelling process, a FEM software namely Plaxis was used. Plaxis can model many geotechnical problems such as bearing capacity, seepath, slope stability, and seismic problems. The outline of FEM framework of Plaxis is given in the Appendix-A with several fundamental sections: 1) Strong form of mechanical problems; 2) Derive weak form from strong form; 3) Shape function matrix elements; 4) Derivation of system equations.

One of the essential elements provided by Plaxis is the Interface/joint elements. This interface element can be used to simulate the region when exists large variation of material stiffness such as

between pile and soil. This element is essential because in some cases the large relative displacement at these regions may affect on the results of simulation. Interface element in Plaxis was based on the concept of zero thickness element proposed by Goodman, Taylor et al. (1968) and Van Langen and Vermeer (1991) with assuming the along and normal stiffness with the interface (k_s and k_n, respectively). The strength along surface also control by Morh Coloumb model with internal friction and cohesion at the interface element (ϕ_c and c_c, respectively).

Several algorithms to enhance convergence rate of elasto-plastic simulations were incorporated in Plaxis such as: arch-length control by Riks (1979); over-relaxation and extrapolation by Vermeer and Langen (1989); and the automatic step size procedure by Van Langen and Vermeer (1990). Furthermore, Plaxis allows user to implement their constitutive model named USDM. USDM can be programed in Fortran language and compiled as a Dynamic Link Library. USDM is called for each gauss points at each increment. At the start of each increment, previous stresses, previous solution-dependent state parameters, strain and time increments are provided by Plaxis. The USDM with a constitutive model will determine the update stresses and state variables.

1.2 Research objectives

The main targets of this study are: 1) to establish a rational constitutive model of crushable soils which incorporates the effect of packing density; 2) to conduct numerical simulations with implementation of the proposed model to examine the effect of packing density on the response of pile. Thus, there are several breakdown tasks to achieve the above targets:

1. To establish relationship between mean coordination number and density. (*Chapter 2*)
2. To establish an evolution law of grading index considering the effect of density through the mean coordination number. (*Chapter 2*)
3. To develop a constitutive model incorporating the proposed evolution law. (*Chapter 2*)
4. To validate the proposed model with an extensive series of elementary tests. (*Chapter 3*)
5. To discuss the breakage responses of the proposed model under different stress paths. (*Chapter 4*)
6. To perform numerical simulation incorporating the proposed model to examine the responses of pile on crushable soils with the effect of density. (*Chapter 5*)

1.3 Outline of dissertation

Chapter 1 Introduction

Research background and research objectives of this study are described in this chapter including the outline of this dissertation

Chapter 2: A constitutive model for crushable soils considering packing density

In this chapter, the effect of packing density on the crushing behavior of the crushable soils is examined through the relationship with mean coordination number. Based on the studies of the systematic packings and experimental results of random packing, a general function described relationship between the mean coordination number and density is proposed. Next, the evolution law of grading index reasonably combines the increase in the coordination number due to an increase packing density, and the increase in the crushing resistance due to the increase in the coordination number. The effect of particle crushing on the stress-strain response is incorporated in the proposed model by lowing the critical state specific volume with the changing grading due to crushing.

Chapter 3: Validations and discussion of soil constitutive model for crushable soils considering packing density

In this chapter, the validity of the proposed constitutive model was verified by comparing the simulation results with an extensive series of elementary tests such as: 1D consolidation tests; isotropic consolidation test (IC); consolidated undrained triaxial test (CD); consolidated drained triaxial test (CU). Subsequently, parametric studies are performed to examine the effect of packing density on the breakage responses of the proposed model under different stress paths.

Chapter 4: Numerical simulation of pile's responses on crushable soil

In this chapter, the implementation of the proposed model into FEM software of Plaxis is verified with elementary model. Then, the simulation incorporated the proposed model is performed to study the response of pile on crushable soils. The simulation results are compared with previous experimental results.

Chapter 5: Concluding and future research

Chapter 5 concludes the substantive findings and novelty of this research and provides the prospects for future research.

1.4 Notations and symbols

As for the notations and symbols, bold letters denote vectors and matrices; "·" denotes an inner product of two vectors (e.g., $\mathbf{a} \cdot \mathbf{b} = a_i b_i$) or a single contraction of adjacent indices of two tensors (e.g., $(\mathbf{c} \cdot \mathbf{d})_{ij} = c_{ik} d_{kj}$); ":" denotes an inner product of two second-order tensors (e.g., $\mathbf{c}: \mathbf{d} = c_{ij} d_{ij}$) or a double contraction of adjacent indices of tensors of rank two and higher (e.g., $(\mathbf{e}: \mathbf{c})_{ij} = e_{ijkl} c_{kl}$); $\otimes$ denotes a tensor product of two vectors (e.g., $(\mathbf{a} \otimes \mathbf{b})_{ij} = a_i b_j$) or a tensor product of two second-order tensors (e.g., $(\mathbf{c} \otimes \mathbf{d})_{ijkl} = a_{ij} b_{kl}$); "‖ ‖" denotes the norm of a first-order tensor (e.g., $\|\mathbf{a}\| =$

$\sqrt{\mathbf{a} : \mathbf{a}} = \sqrt{a_i a_i}$) or a second-order tensor (e.g., $\|\mathbf{c}\| = \sqrt{\mathbf{c} : \mathbf{c}} = \sqrt{c_{ij} c_{ij}}$); $\mathbf{1}$ is the second-order identity tensor; $\mathbf{I}$ is the fourth-order identity tensor $\left(I_{ijkl} = \frac{1}{2} \left(\delta_{ik} \delta_{jl} + \delta_{il} \delta_{jk} \right) \right)$; " $\dot{}$ " denotes the time derivative; and the subscript zero denotes the initial state (e.g., e_0 = initial void ratio).

Chapter 2 : A constitutive model for crushable soil considering packing density

2.1 Relationship between packing density and coordination number

2.1.1 Packing density effect on particle crushing through coordination number

The densely packed soils have more coordination numbers (the number of contact points) in each particle as compared to the loosely packed soils. Thus, the stress distribution on each particle (average contact stress) is lesser for denser soils. Hence, these denser soils are more resistant to crushing. Due to less coordination number, the crushing mode of a loosely packed soils is more likely splitting mode while it is chipping mode for densely packed soils (Fig. 2-1) (Valdes 2003, Guimaraes, Valdes et al. 2007). Supported by SEM-images of particle crushing after 1D consolidation tests, Guimaraes, Valdes et al. (2007), showed that the particles of the denser soils tended to exhibit several chips on their surface, meanwhile, the particles of the looser soils seemed to have more likely to have splitting mode (Fig. 2-1). Thus, coordination number of different packing densities is a key factor effect the breakage response.
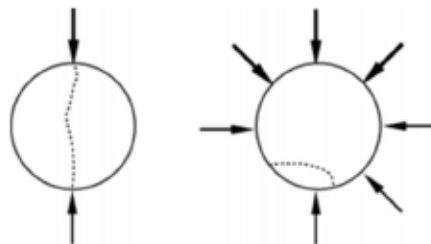
Figure 2-1: Failure modes with different coordination number (Guimaraes, Valdes et al. 2007)
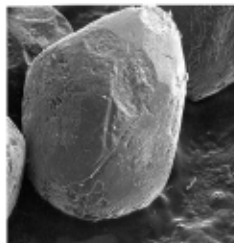
Figure 2-2: SEM image of densely packed soil (Guimaraes, Valdes et al. 2007)

2.1.2 Systematic packing and experimental results

Conventionally, the denser soils have higher coordination number as compared to the looser soil. As the density of soils increases, their coordination numbers also increase correspondingly. Thus, a relationship between the density and the coordination number is feasible. Also, a simple relationship between the density and coordination number can help to evaluate the variations of the coordination number easily. For that purpose, systematic packings of uniform spheres and experimental results of random packing (Oda 1977, Matsushima, Uesugi et al. 2008) are examined in this study to identify this relationship. The systematic packing or the order packing of uniform spheres have been studied extensively by many researchers (Graton and Fraser 1935, Aïm and le Goff 1968, Haughey and Beveridge 1969, German and Munir 1975, German 1989, German 2014, Patankar and Mandal 2014). In order to simplify and classify each packing type for the systematic packing, eight typical patterns have been identified in table 2-1. For example, a simple cubic packing (shown in Fig. (2-3)) can be decomposed into two contact patterns of S1 and S4. Therefore, the simple cubic packing type is denoted as a combination of "S1+S4+S1" and the coordination number of the combination is 6. Similarly, the packing types, combination, coordination number and corresponding void ratio are finally enlisted in the table 2-1. As coordination number increases, the void ratio reduces correspondingly.

A wide range of data from systematic packings of uniform spheres (table. 2-2) to random packings of glass beads (Oda 1977), Toyoura sand and glass beads (by X-ray CT test of Matsushima, Uesugi et al. (2008)) have been portrayed in Fig. (2-4) to demonstrate the similarity trend between coordination number and void ratio. Due to the variations in distribution of the coordination number in each particle for a random packing, the coordination number is presented as the mean coordination number, C_N. Based on the common trend between the mean coordination number, C_N, and void ratio, e, a simple relationship is proposed as follow:

$$C_N = \frac{C_{N\max}}{1+be^{k^*}} \qquad (2\text{-}1)$$

where $C_{N\max}$ is the maximum coordination number in the case of the full density (the void is fully occupied by the solid's particles). Identified by other researchers (Beresford 1969, Bouvard and Lange

1991), the maximum coordination number, $C_{N\max}$, can reach to the maximum value of 15. b and k are material constants which can be determined by curve fitting method. For example, a set of parameters of $C_{N\max} = 14$, $b = 1.23$ and $k^{\bullet} = 1.4$ is the best fit for the data of systematic packings, whereas, a set of parameters of $C_{N\max} = 14$, $b = 2.00$ and $k^{\bullet} = 1.4$ is the best fit for the experimental data by Oda (1977).

Table 2-1. Two-dimensional basic contact patterns of the systematic packing

Contact pattern	Description	Number of contact	ID
	Single contact	1	S1
	Double contacts	2	S2
	Double contact (separated contact)	2	SN2
	Triple contacts	3	S3
	Triple contacts (separated contact)	3	SN3
	Four contacts	4	S4
	Six contacts	6	S6
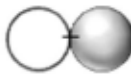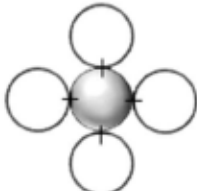
Packing type	Identify contact patterns	Combination	Coordination number
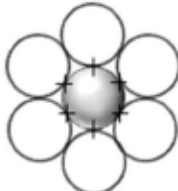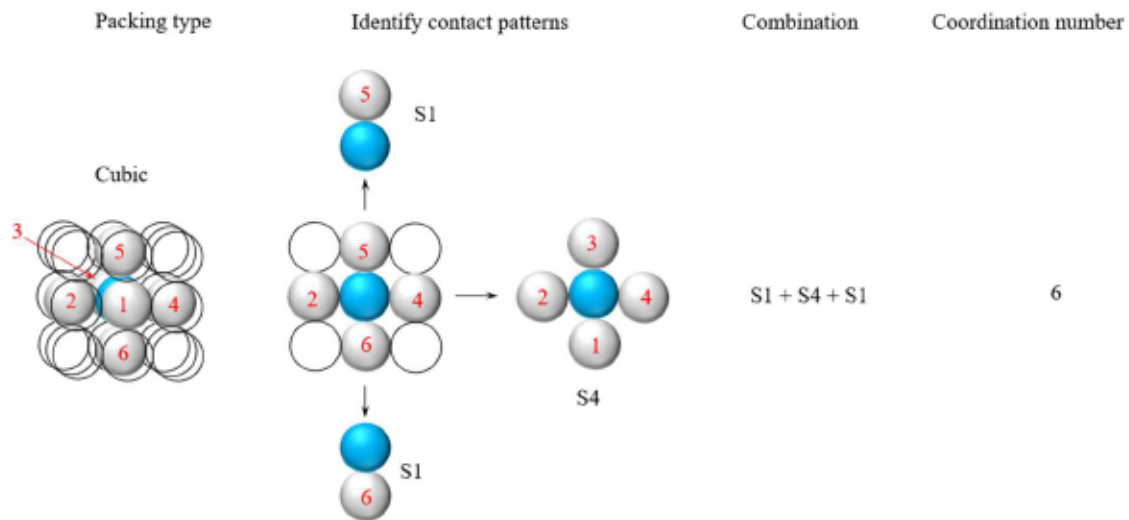
Figure 2-3: Decomposition of a cubic packing

Table 2-2. Contact patterns of the systematic packing

Packing type	Combination	Coordination number	Void ratio
Rhombohedral	S3+S6+S3	12	0.350
	S3+S6+S2	11	0.404
Tetragonal-sphenoidal	S2+S6+S2	10	0.432
	S2+S6+S1	9	0.630
Orthorhombic	S2+S4+S2	8	0.470
Hexagonal	S1+S6+S1	8	0.654
	S2+S4+S1	7	0.782
Cubic	S1+S4+S1	6	0.910
	SN3+SN2	5	1.481
Diamond	SN3+S1	4	1.940
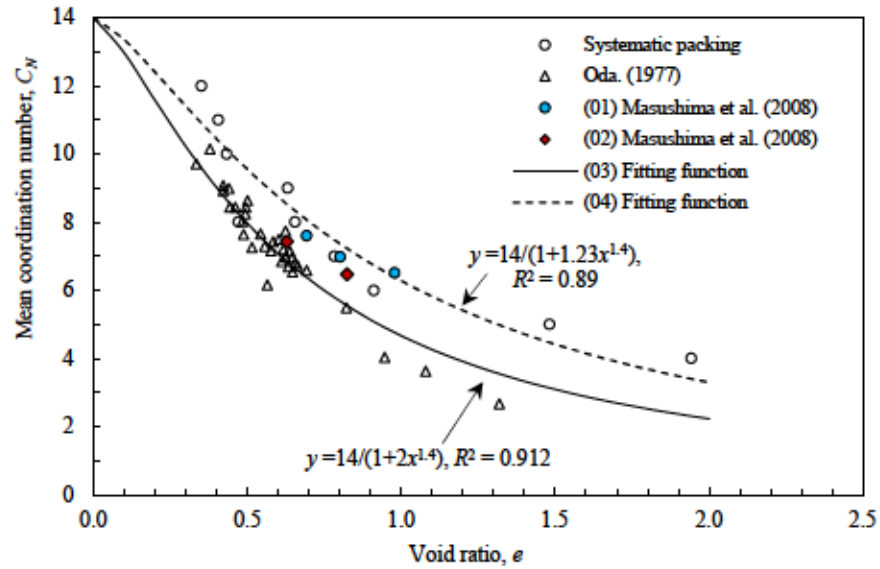
Figure 2-4: Functional relations between mean coordination number and void ratio. (01) and (2) X-ray CT for Toyoura sand and glass beads, respectively (Matsushima, Uesugi et al. 2008); (03) and (04) are fitting functions for experimetal data of Oda (1977) and systematic packing data, respectively.

2.1.2 Evolution law of grading index I_G

From identification the relationship between the mean coordination number, C_N, and void ratio, e, any variation of the mean coordination number can be easily obtained through the relationship with void ratio. The relationship is crucial because the breakage response of the crushable soils can be evaluated by the variations of the coordination number. In order to bring these fundamental factors into a constitutive model, a new evolution rule is proposed by incorporating stress state and the mean coordination number.

As described in Eq. (1-1), the grading index, I_G, depends only on the crushing stress, p_x, which is composed by stresses (p',q) only. Thus, the former function described the evolution of grading index through the variation of stresses only. Without considering coordination number, the effect of density was omitted in the former function (Kikumoto, Wood et al. 2010). A similar form of Eq. (1-1) is a function of fracture probability, p_f, derived by McDowell, Bolton et al. (1996) based on the Weibull statistics as follows:

$$p_f = 1 - \exp\left\{-\left(\frac{d}{d_o}\right)^3 \left(\frac{\bar{\sigma}}{\sigma_o}\right)^m \left(\frac{1}{C-2}\right)^a\right\} \tag{2-2}$$

where d and d_o are the current particle size and the initial particle size, respectively. $\bar{\sigma}$ is the macroscopic stress, σ_o is the tensile stress such that 37% of total number of test block survive, C is the coordination number, m and a are material constants. Both Eqs. (1-1) and (2-2) have similar form of exponential function and both grading index and facture probability are the indicators of particle crushing. It is noted that the difference in Eqs. (1-1) and (2-2) is the fracture probability function, Eq. (2-2), incorporating the coordination number, C, as a factor controlling particle breakage. Therefore, as showing Eq. (2-2), the higher coordination number each particle has, the more resistance for grain is against crushing.

During volumetric compression, soil state tends to be denser inducing higher mean coordination number. Therefore, the higher resistance is obtained against crushing. The limitation of Eq. (1-1) is that the resistance stress, p_r, is a constant value, whereas, it should be a variable dependent upon the mean coordination number, C_N. Recognizing such limitation, the new crushing resistance is revised as:

$$p_r = p_{r|C_N=3}\,(C_N - 2)^{\frac{a}{n}} \tag{2-3}$$

where $p_{r|C_N=3}$ is the crushing resistance stress, p_r, when the mean coordination number, C_N, is 3. α is material constant to control the rate of crushing resistance. Hereafter, whenever the mean coordination number, C_N, increases, the crushing resistance stress, p_r, also increases correspondingly. Substituting Eq. (2-3) into Eq. (1-1), the function of grading index, I_G, incorporating the mean coordination number, C_N, can be derived as:

$$I_G = 1 - \exp\left\{-\left(\frac{p_x - p_{x0}}{p_{r|C_N=3}}\right)^n \left(\frac{1}{C_N - 2}\right)^a\right\} \tag{2-4}$$

As particle crushing is an irreversible process, the function of grading index Eq. (2-4) is also required to capture the phenomenon. For that purpose, a maximum crushing stress, p_{xc}, which records

the maximum value of crushing stress with respect to the mean coordination number, C_N, from the beginning iteration to the current state, is defined as:

$$p_{xc} = \max \left\{ \left| \frac{p_x - p_{xo}}{(C_N - 2)^{\frac{\alpha}{n}}} \right| \right\} \qquad (2\text{-}5)$$

Substituting Eq. (2-5) into Eq. (2-4), a function of grading index can be finally derived as:

$$I_G = 1 - \exp\left\{ -\left(\frac{p_{xc}}{p_{rCN}} \right)^n \right\} \qquad (2\text{-}6)$$

Function of grading index (Eq. (2-6)) plays an importance role in describing the irreversible relationship between grading index, stresses and coordination number. Based on this function, the evolution rule of grading index can be obtained by taking time derivative:

$$\dot{I}_G = \frac{\partial I_G}{\partial p_{xc}} \dot{p}_{xc} \qquad (2\text{-}7)$$

Based on definition of the maximum crushing stress, p_{xc}, the variation of maximum crushing stress, $\dot{p}_{xc}$, also a non-negative value. Thus, this satisfies the requirement of variation of grading index, $\dot{I}_G$, (Eq. (2-7)) being also a non-negative value. Therefore, simple proposing of the maximum crushing stress function (Eq. (2-5)), the function and evolution of grading index (Eqs. (2-6) and (2-7)) can capture the irreversible responses of the crushable soil.

From Eq.(2-5), the variation of the maximum stress, $\dot{p}_{xc}$, can be determined:

$$\dot{p}_{xc} = \begin{cases} \dfrac{\partial p_{xc}}{\partial p_x} \dot{p}_x + \dfrac{\partial p_{xc}}{\partial C_N} \dot{C}_N & \text{when } p_{xc} = p_{xccurrent}, \dot{p}_{xc} > 0 \\ 0 & \text{when } p_{xc} < p_{xccurrent}, \dot{p}_{xc} = 0 \end{cases} \qquad (2\text{-}8)$$

where $p_{xccurrent} = \dfrac{p_x - p_{xo}}{(C_N - 2)^{\frac{\alpha}{n}}}$ is the current crushing stress at corresponding mean coordination number.

It can be interpreted from Eqs. (2-7) and (2-8) for the crushing conditions as:

31

1) The particle crushing occurs ($\dot{I}_G > 0$) when the maximum crushing stress, p_{xc}, is equal to the current crushing stress at the corresponding mean coordination number, $p_{xccurrent}$ and the variation of maximum crushing stress, $\dot{p}_{xc}$, is positive ($p_{xc} = p_{xccurrent}$ and $\dot{p}_{xc} > 0$).

2) No particle crushing occurs ($I_G = 0$) when the maximum crushing stress, p_{xc}, is higher than the current crushing stress at the corresponding mean coordination number, $p_{xccurrent}$ and the variation of maximum crushing stress, $\dot{p}_{xc}$, is zero ($p_{xc} < p_{xccurrent}$ and $\dot{p}_{xc} = 0$)

2.1.2 Formulation of the crushing stress, p_x

As reported by many researchers (Lee and Farhoomand 1967, Hardin 1985, Lade, Yamamuro et al. 1996, Nakata, Hyodo et al. 2001), the stress state (stress level, stress magnitude, and the stress path) were a key factor controlling the breakage responses of the crushable soils. In this study, the stress effect is described by the crushing stress, p_x, (a combination of the mean effective stress, p', and deviator stress, q) which controls the breakage responses through Eqs. (2-5) and (2-8). Based on experimental evidences (Hardin 1985), the crushing stress function as a composition of effective octahedral normal and shear stress was derived. Then, it was further derived into a combination of mean effective stress, p', and deviator stress, q by Kikumoto, Wood et al. (2010). Based on these studies, a similar simple form of crushing stress, p_x, is proposed:

$$p_x = p\left\{1 + \left(\frac{q}{M_x p}\right)^3\right\} \tag{2-9}$$

where M_x is the constant parameter which controls the effect of deviator stress and mean effective stress. A crushing stress surface, f_x, is obtained by arranging Eq.(2-9) as:

$$f_x = P_x - p\left\{1 + \left(\frac{q}{M_x p}\right)^3\right\} \tag{2-10}$$

As illustrated in Fig. (2-5), the shape of the crushing surface is more broaden when M_x increases. Thus, the parameter M_x is also used to control the shape of the crushing surface. From Eq. (2-10), the variation of the crushing stress can be derived as:

$$\dot{p}_x = \frac{\partial f_x}{\partial \sigma'} \dot{\sigma}' \qquad (2\text{-}11)$$

Overcoming former limitations in the evolution rule of grading index, the proposed evolution rule (Eqs. (2-7) and (2-8)) take account of the stress change and the variation in the mean coordination number. Furthermore, any variation in density, correspondently, lead to the change in the mean coordination number (Eq. (1-1)). Then, the change in the mean coordination number can affect the crushing responses (Eqs. (2-7) and (2-8)). Therefore, the effect of density on breakage behavior can be examined by the proposed evolution rules.
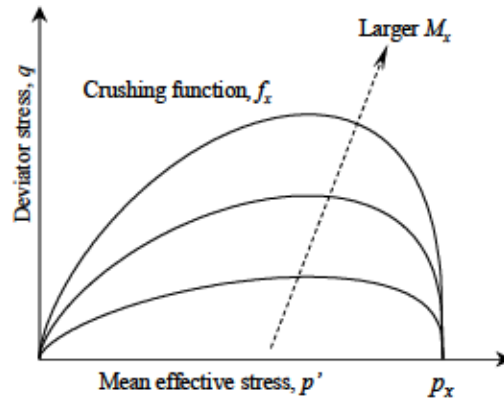
Figure 2-5: Variations of crushing surface with the change of M_x

2.1.3 Formulation of the crushing stress, p_x

Based on the simple relationship between density, e, and the mean coordination number, C_N, in Eq.(1-1), any variation in the mean coordination number leads to the change in density, correspondently. Also, variation in density, $\dot{e}$, can make the strain change, $\dot{\varepsilon}$. Therefore, the variation of the mean coordination, $\dot{C}_N$, can be derived as:

$$\dot{C}_N = \frac{C_N{}^2 bk^* \dot{e}^{k^*-1}(v_o 1 : \dot{\varepsilon})}{C_{N\text{max}}}$$
(2-12)

where $\dot{e} = v_o \dot{\varepsilon}_v$ and $\dot{\varepsilon}_v = 1 : \dot{\varepsilon}$

when crushing occurs $(\dot{I}_G > 0)$, the evolution of the maximum crushing stress can be derived by substituting Eqs. (2-11) and (2-12) into Eq. (2-8) as:

$$\dot{p}_{xc} = \frac{1}{(C_N - 2)^{\frac{\alpha}{n}}} \frac{\partial f_x}{\partial \sigma'} \dot{\sigma}' - \frac{\alpha p_{xc}}{n(C_N - 2)} \frac{C_N{}^2 bk^* \dot{e}^{k^*-1}(v_o 1 : \dot{\varepsilon})}{C_{N\text{max}}}$$
(2-13)

Substituting Eqs. (2-6) and (2-12) into Eq.(2-7) to obtain the variation of grading index, $\dot{I}_G$, when crushing occurs

$$\dot{I}_G = A_1 \frac{\partial f_x}{\partial \sigma'} \dot{\sigma}' + A_2 1 : \dot{\varepsilon}$$
(2-14)

Where

$$A_1 = \frac{(1 - I_G)}{(C_N - 2)^{\frac{\alpha}{n}}} \frac{n}{p_{xc}} \left(\frac{p_{xc}}{P_r} \right)^n$$
(2-15)

$$A_2 = \frac{(1 - I_G)}{(C_N - 2)} \frac{C_N{}^2 bk^* \dot{e}^{k^*-1} v_o}{C_{N\text{max}}}$$
(2-16)

2.2 A constitutive soil model considering particle crushing

The core idea of the proposed model is established on a state boundary surface (SBS) originated from definition of an available strength , η_u , in Servent-trend sand model (Gajo and Muir Wood 1999, Gajo and Muir Wood 1999). Meanwhile, the fundamental framework of the proposed model is based on continuum mechanics incorporating the effect of particle crushing.

2.2.1 State boundary surface (SBS)

As reported by many researchers (Daouadji, Hicher et al. 2001, Muir Wood and Maeda 2007, Bandini and Coop 2011, Ghafghazi, Shuttle et al. 2014), particle crushing leads to a denser state of soil and cause a downward parallel shift in the CSL in $e - \log p$ space. Thus a new state parameter, ψ_c, representing the downward shift of SCL is introduced into a conventional form of SCL for sand (Gajo and Muir Wood 1999) as:

$$v_{cs} = \Gamma - \lambda \ln \frac{p'}{p_a} - \psi_c \qquad (2\text{-}17)$$

where v_{cs} is the specific volume at the critical state, p_a is the atmospheric pressure, ψ_c ($0 \leq \psi_c \leq \xi$) is a non-negative variable defined as the volumetric distance between the CSL at the current grading and the limit grading ($I_G = 1$). ξ is the volumetric distance between the CSL at the unit grading ($I_G = 0$) and the limit grading ($I_G = 1$) (indicated in Fig.(2-6)). Γ defines as the specific volume at the critical state when $p' = p_a$ and $\psi_c = 0$.

Recognizing that the current state of soil (dense or loose) governing stress-strain behavior, a state parameter for sand (Been and Jefferies 1985), ψ_s, defined as the volumetric distance of the current specific volume, v, from the current SCL at the current mean effective stress, p' was presented as:

$$\psi_s = v - v_{cs} \qquad (2\text{-}18)$$

Having identified the state parameter for sand, ψ_s, the Severnt-Trent sand model (Gajo and Muir Wood 1999) further introduced the available strength, η_u, in order to control the evolution of strength. The variable strength, η_u, is proposed to be upper limit of the current strength, η. Also, it is assumed to be a variable dependent upon the state parameter, ψ_s.

$$\eta \leq \eta_u (\psi_s) \qquad (2\text{-}19)$$
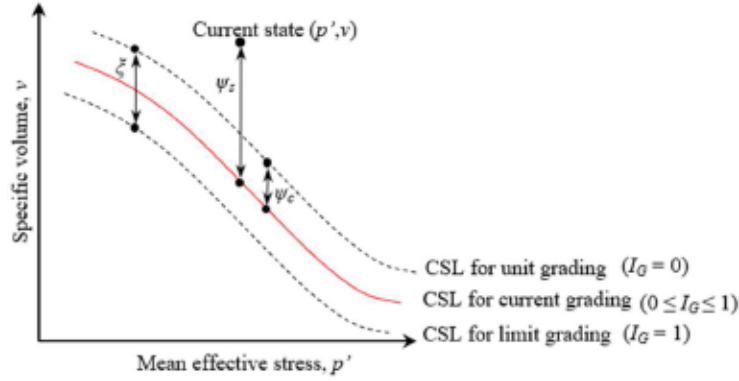
Figure 2-6: Critical state line in $p'-v$ plane for the crushable soils
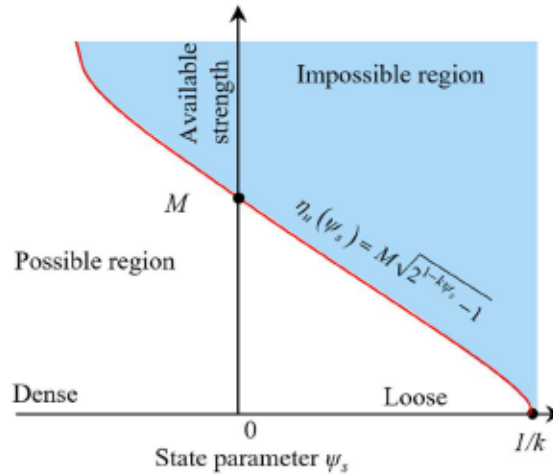
Figure 2-7: The Proposed non-linear available strength function of state parameter

In this study, a similar non-linear relationship shown in Fig. (2-7) between the available strength and the state parameter, ψ_s, is proposed as:

$$\eta_u(\psi_s) = M\sqrt{2^{1-k\psi_s}-1} \tag{2-20}$$

where k is a positive constitutive parameter.

From definition of the available strength, η_u, the possible and impossible regions are identified (Fig. (2-7)). The available strength, η_u, plays a role as a threshold of these regions. Substituting Eqs. (2-17), (2-18), and (2-20) into Eq. (2-19), an alternative expression for Eq.(2-19) is derived as the upper threshold of specific volume, v_u, for sand.

$$v \leq v_u = \frac{1}{k} + \Gamma - \lambda \ln\frac{p'}{p_a} - \frac{1}{k}\frac{\ln\left\{1+\left(\frac{\eta}{M}\right)^2\right\}}{\ln 2} - \psi_c \qquad (2\text{-}21)$$

here, the upper specific volume, v_u, is defined as the loosest state of soil at the current stress (p',η) and the current state parameter, ψ_c. It is noted that Eq.(2-21) also separates the possible and impossible states in space of the effective stress, p', stress ratio $,\eta$, and specific volume, v. Thus, a unique state boundary surface (SBS) is also found for sand. The SBS plays a central role in describing soil behavior in the proposed model.

2.2.2 Elasto-plastic model for sand

For the stress-strain relationship, an additive decomposing of the total strain rate tensor, $\dot{\varepsilon}$, is assumed as follows:

$$\dot{\varepsilon} = \dot{\varepsilon}^e + \dot{\varepsilon}^p \qquad (2\text{-}22)$$

where $\dot{\varepsilon}^e$ and $\dot{\varepsilon}^p$ are elastic and plastic strain rate tensors, respectively.

Elastic volumetric behavior is assumed to follow a conventional, linear relationship in the semi-logarithmic plane of $\ln p'$ and v. Thus an elastic part of the variation in the specific volume, dv^e, is given as:

$$dv^e = -\kappa\frac{dp'}{p'} \qquad (2\text{-}23)$$

where κ is the swelling index that represents the slope of the isotropic unloading (swelling) line in the $\ln p'-v$ plane. From Eq. (2-23), the nonlinear elastic bulk modulus can be defined as:

$$K = \frac{v_0}{\kappa}p' \qquad (2\text{-}24)$$

Assuming that Poisson's ratio $,v_e$, is constant, the shear modulus, G, is:

$$G = \frac{3K(1-2v_e)}{2(1+v_e)} \qquad (2\text{-}25)$$

Thus, the incremental isotropic elastic relationship is:

$$\dot{\sigma}' = D^e : \dot{\varepsilon}^e \qquad (2\text{-}26)$$

Where $\dot{\sigma}'$ is the rate of effective stress tensor and D^e is the elastic stiffness tensor derived as:

$$D^e = \left\{ K\mathbf{1} \otimes \mathbf{1} + 2G\left(I - \frac{1}{3}\mathbf{1} \otimes \mathbf{1} \right) \right\} \qquad (2\text{-}27)$$

The change in specific volume never exceeds beyond the SBS during plastic volumetric deformation. Thus, a bounding surface, $\tilde{f}$, can be established as:

$$\tilde{f} = v - v_u \leq 0 \qquad (2\text{-}28)$$

Similar to yielding surface in classical critical state model, the non-positive bounding surface, $\tilde{f}$, increases to zero value when the state of soil approaches the SBS. Within the yielding surface, the classical model predicts purely elastic behavior whereas actual sand exhibits elastoplastic irreversible deformation. Therefore, in order to describe a smooth transition from elastic to elastoplastic states, a yield surface within the bounding surface is assumed in the proposed model. Accordingly, a state parameter of volumetric difference, Ω, from the current specific volume to the specific volume on the SBS is presented to scale the current state to the normal yielding (bounding) surface.

$$\Omega = v_u - v \qquad (2\text{-}29)$$

Based on Eqs. (2-28) and (2-29), the yield surface can be derived as:

$$f = v - v_u + \Omega \equiv 0 \qquad (2\text{-}30)$$

Here, the yield function is identically equal to zero.

The variables $\left(v, p', \eta, \varepsilon_v^p, \Omega, \psi_c \right)$ are hereafter denoted as $\left(v_o, p'_o, \eta_o, \varepsilon_{vo}^p(=0), \Omega_o, \psi_{co} \right)$ at initial state and $\left(v, p', \eta, \varepsilon_v^p, \Omega, \psi_c \right)$ at the current state. The variation in specific volume from the initial state to the current state, Δv, can be decomposed into elastic and plastic variations in the specific volume, Δv^e and Δv^p

$$\Delta v = v - v_o \tag{2-31}$$

$$\Delta v = \Delta v^e + \Delta v^P = -\kappa \ln \frac{p'}{p'_o} - v_o \varepsilon_v^P \tag{2-32}$$

where $\varepsilon_v^P (= tr\varepsilon^P)$ denotes the plastic volumetric strain. Substituting Eqs. (2-21), (2-31) and (2-32) into Eq. (2-30), the yielding surface can be revised as:

$$f\left(v, p', \eta, \varepsilon_v^P, \Omega, \psi_c\right) = v_o - \kappa \ln \frac{p'}{p'_o} - v_o \varepsilon_v^P - \left[\frac{1}{k} + \Gamma - \lambda \ln \frac{p'}{p'_a} - \frac{1}{k} \frac{\ln\left\{1 + \left(\frac{\eta}{M}\right)^2\right\}}{\ln 2} - \psi_c\right] + \Omega \equiv 0 \tag{2-33}$$

At initial state $f\left(v_o, p'_o, \eta_o, \varepsilon_{vo}^P (=0), \Omega_o, \psi_{co}\right) \equiv 0$, the specific volume at the critical state, Γ, can be derived from Eq.(2-33) as:

$$\Gamma = v_o - \left[\frac{1}{k} + -\lambda \ln \frac{p'_o}{p'_a} - \frac{1}{k} \frac{\ln\left\{1 + \left(\frac{\eta_o}{M}\right)^2\right\}}{\ln 2} - \psi_{co}\right] + \Omega_o \equiv 0 \tag{2-34}$$

Substituting Eq. (2-34) into Eq. (2-33), a simple form of the yielding surface function is obtained as:

$$f\left(v, p', \eta, \varepsilon_v^P, \Omega, \psi_c\right) = (\lambda - \kappa) \ln \frac{p'}{p'_o} + \frac{1}{k} \ln\left\{\frac{1 + \left(\frac{\eta}{M}\right)^2}{1 + \left(\frac{\eta_o}{M}\right)^2}\right\} + (\Omega - \Omega_o) + (\psi_c - \psi_{co}) - v_o \varepsilon_v^P \equiv 0 \tag{2-35}$$

As the soil does not exhibit any dilation in the critical state $(\eta = M)$ and further assumption of associated flow, the following condition is obtained:

$$\left.\frac{\partial f}{\partial p'}\right|_{\eta = M} = 0 \tag{2-36}$$

Substituting Eq. (2-36) in Eq. (2-35), Eq. (2-35) can be reduced to:

$$\frac{1}{k} = \lambda - \kappa \tag{2-37}$$

Finally, the yield surface function can be obtained by substituting Eq. (2-37) back into Eq. (2-35).

$$f\left(v, p', \eta, \varepsilon_v^p, \Omega, \psi_c\right) = (\lambda - \kappa)\ln\frac{p'\left\{1 + \left(\dfrac{\eta}{M}\right)^2\right\}}{p'_o\left\{1 + \left(\dfrac{\eta_o}{M}\right)^2\right\}} + (\Omega - \Omega_o) + (\psi_c - \psi_{co}) - v_o \varepsilon_v^p \equiv 0 \qquad (2\text{-}38)$$

In any loading path, the Kuhn-Tucker conditions (Kuhn and Tucker 1951) must be satisfied.

$$f \leq 0; \quad \dot{\Lambda} \geq 0; \quad f\dot{\Lambda} = 0 \qquad (2\text{-}39)$$

where $\dot{\Lambda}$ is plastic multiplier

As the yield function in the proposed model Eq. (2-38) is identically equal to zero, the loading condition reduces to:

$$\dot{\Lambda} \geq 0 \qquad (2\text{-}40)$$

where $\dot{\Lambda} = 0$ indicates elastic behavior (neutral or unloading) and $\dot{\Lambda} > 0$ indicates plastic deformation (loading).

When soil state at the yield surface, the consistency condition, that is the time derivative of the yield function $f\left(v, p', \eta, \varepsilon_v^p, \Omega, \psi_c\right)$ equal zero must be satisfied.

$$\dot{f} = \frac{\partial f}{\partial \sigma'}\dot{\sigma}' + \frac{\partial f}{\partial \varepsilon_v^p}\dot{\varepsilon}_v^p + \frac{\partial f}{\partial \Omega}\dot{\Omega} + \frac{\partial f}{\partial \psi_c}\dot{\psi}_c \equiv 0 \qquad (2\text{-}41)$$

As assumption of associated flow, the hardening rule for the plastic volumetric strain, ε_v^p, is:

$$\frac{\partial f}{\partial \varepsilon_v^p}\dot{\varepsilon}_v^p = -v_o \dot{\Lambda} tr \frac{\partial f}{\partial \sigma'} \qquad (2\text{-}42)$$

From definition of the state parameter of volumetric distance, Ω, as a margin from the current state to the normal yield (bounding) surface, it must decrease with the development in plastic deformation and converge to zero. Consequently, when soil exhibits plastic deformation, a simple decay function is proposed for the evolution of Ω:

40

$$\frac{\partial f}{\partial \Omega} \dot{\Omega} = -\omega \Omega |\Omega| \|\dot{\varepsilon}^p\| \qquad (\dot{\Lambda} > 0) \tag{2-43}$$

Where ω is a parameter that controls the rate of evolution of Ω.

If the soil exhibits purely elastic deformation (unloading or neutral), the consistency condition (Eq.(2-41)) still needs to be satisfied as the yield function, f, is identically equal to zero. Also, no plastic deformation, $\dot{\varepsilon}_v^p = 0$, and no particle crushing occurrence, $\dot{\psi}_c = 0$, in the unloading or neutral conditions, the evolution law of Ω can be derived from Eq.(2-41) as:

$$\dot{\Omega} = -\frac{\partial f}{\partial \sigma'} \dot{\sigma}' \qquad (\dot{\Lambda} = 0) \tag{2-44}$$

Evidently, particle crushing leads to a denser state of soil (Fig. (2-6)). The occurrence of particle crushing can increase the grading index, I_G (from 0 to 1), and decrease the current specific volume through the state parameter of crushing, ψ_c (from 0 to ξ), respectively. Therefore, a simple linear relationship for the state parameter of crushing, ψ_c, is defined as:

$$\psi_c = \xi I_G \tag{2-45}$$

Identifying the relationship between the state parameter of crushing, ψ_c, and grading index, I_G, the evolution rule for ψ_c can easily be obtained as:

$$\frac{\partial f}{\partial \psi_c} \dot{\psi}_c = \xi \dot{I}_G \tag{2-46}$$

When no crushing occurs $\left(\dot{I}_G = 0 \right)$, the current crushing stress at the current density is smaller than the maximum crushing stress. Also, there is no stress change in the maximum crushing stress ($p_{xc} < p_{xccurrent}$ and $\dot{p}_{xc} = 0$). From the Eqs. (2-41), (2-42), (2-43), and (2-46) , the magnitude of plastic strain rate, $\dot{\Lambda}$, is derived as:

$$\dot{\Lambda} = \left\langle \frac{\dfrac{\partial f}{\partial \sigma'} : D^e : \dot{\varepsilon}}{v_0 tr \dfrac{\partial f}{\partial \sigma'} + \omega \Omega |\Omega| \left\| \dfrac{\partial f}{\partial \sigma'} \right\| + \dfrac{\partial f}{\partial \sigma'} : D^e : \dfrac{\partial f}{\partial \sigma'}} \right\rangle \tag{2-47}$$

When the rate of the plastic multiplier is positive ($\dot{\Lambda} > 0$), the rate form of the elastoplastic stress-strain relationship is converted to:

$$\dot{\sigma}' = D^{ep} : \dot{\varepsilon} = \left(D^e - \frac{D^e : \dfrac{\partial f}{\partial \sigma'} \otimes \dfrac{\partial f}{\partial \sigma'} : D^e}{v_o tr \dfrac{\partial f}{\partial \sigma'} + \omega \Omega |\Omega| \left\| \dfrac{\partial f}{\partial \sigma'} \right\| + \dfrac{\partial f}{\partial \sigma'} : D^e : \dfrac{\partial f}{\partial \sigma'}} \right) : \dot{\varepsilon} \qquad (2\text{-}48)$$

Where D^{ep} is the elasto-plastic stiffness tensor.

When particle crushing occurs $\left(\dot{I}_G > 0 \right)$, the current crushing stress at the current density is equal to the maximum crushing stress. Also, there is stress change in the maximum crushing stress $(p_{xc} = p_{xccurrent}$ and $\dot{p}_{xc} > 0)$. As described in appendix and from Eq.(2-46), the evolution rule for ψ_c can be presented as:

$$\frac{\partial f}{\partial \psi_c} \psi_c = \xi \left(A_1 \frac{\partial f_x}{\partial \sigma'} : \sigma' + A_2 1 : \dot{\varepsilon} \right) \qquad (2\text{-}49)$$

From Eqs. (2-41), (2-42), (2-43), and (2-49), the magnitude of plastic strain rate, $\dot{\Lambda}$, is derived as:

$$\dot{\Lambda} = \left\langle \frac{\left\{ \left(\dfrac{\partial f}{\partial \sigma'} + \xi A_1 \dfrac{\partial f_x}{\partial \sigma'} \right) : D^e - \xi A_2 1 \right\} : \dot{\varepsilon}}{v_o tr \dfrac{\partial f}{\partial \sigma'} + \omega \Omega |\Omega| \left\| \dfrac{\partial f}{\partial \sigma'} \right\| + \left(\dfrac{\partial f}{\partial \sigma'} + \xi A_1 \dfrac{\partial f_x}{\partial \sigma'} \right) : D^e : \dfrac{\partial f}{\partial \sigma'}} \right\rangle \qquad (2\text{-}50)$$

When the rate of the plastic multiplier is positive ($\dot{\Lambda} > 0$), the rate form of the elastoplastic stress-strain relationship is converted to:

$$\dot{\sigma}' = D^{ep} : \dot{\varepsilon} = \left(D^e - \frac{D^e : \dfrac{\partial f}{\partial \sigma'} \otimes \left(\dfrac{\partial f}{\partial \sigma'} + \xi A_1 \dfrac{\partial f_x}{\partial \sigma'} \right) : D^e - D^e : \dfrac{\partial f}{\partial \sigma'} : 1 \xi A_2}{v_o tr \dfrac{\partial f}{\partial \sigma'} + \omega \Omega |\Omega| \left\| \dfrac{\partial f}{\partial \sigma'} \right\| + \left(\dfrac{\partial f}{\partial \sigma'} + \xi A_1 \dfrac{\partial f_x}{\partial \sigma'} \right) : D^e : \dfrac{\partial f}{\partial \sigma'}} \right) : \dot{\varepsilon} \qquad (2\text{-}51)$$

42

Chapter 3 : Validation and Discussion of Constitutive Model for Crushable Soils Considering Packing Density

3.1 Purpose

Table 3-1: Material parameters for the simulations by the proposed model

Parameters	Description	Value				
		(1)	(2)	(3)	(4)	(5)
λ	compression index	0.195	0.150	0.150	0.350	0.145
κ	swelling index	0.005	0.010	0.015	0.015	0.001
Γ	specific volume on CSL at $p' = 98$ kPa	2.77	2.20	3.01	4.77	2.00
M	critical state stress ratio	1.13	1.65	1.65	1.65	1.50
v_e	Poisson's ratio	0.2	0.2	0.2	0.2	0.2
ω	parameter for the rate of Ω	1000	200	50	50	200
p_{rCN}	crushing resistance stress (kPa) when $C_N = 3$	1000	1200	2650	5380	2200
M_x	parameter controlling the shape of crushing surface	0.95	0.95	0.95	0.95	1.05
ξ	volumetric distance between SBSs of $I_G = 0$ and $I_G = 1$	0.35	0.55	1.25	1.25	0.55
p_{xo}	initial crushing stress (kPa)	1000	100	50	50	50
n	parameter for the ratio of crushing stress	4.00	1.10	1.55	1.85	1.00
α	parameter for the rate of crushing resistance	8.20	3.00	1.15	2.15	3.00
C_{Nmax}	maximum coordination number	14	14	14	15	14
b	parameter for the e-C_N relationship	2.00	2.00	2.00	0.0035	2.00
k^*	parameter for the e-C_N relationship	1.4	1.4	1.4	9.0	1.4

Note:

(1)   Ottawa sand (Valdes 2003, Guimaraes, Valdes et al. 2007)

(2)   Aio sand (Hyodo, Wu et al. 2017)

(3)   Dogs Bay sand (Altuhafi and Coop 2011)

(4)   Verified with DEM results (Bolton, Nakata et al. 2008)

(5)   HI sand (Shahnazari and Rezvani 2013)

The performance of the proposed model is verified with a wide range of tests, such as, 1D consolidation (Valdes 2003, Guimaraes, Valdes et al. 2007, Altuhafi and Coop 2011), isotropic

consolidation (Hyodo, Wu et al. 2017), consolidated undrained triaxial test (CU) (Hyodo, Wu et al. 2017), and consolidated drained triaxial test (CD) with constant radial stress (Shahnazari and Rezvani 2013). Furthermore, the model responses of the breakable and unbreakable states are compared with the results of Discrete Element Methods (DEM) by Bolton, Nakata et al. (2008). Next, the effects of density on breakage behavior are also examined through the evolutions of the grading index, the mean coordination number and confining stresses. Finally, the non-uniqueness of the critical line is explored by a series of numerical simulations by the proposed model. The material parameters for the validations and discussions are enlisted in the Table 3-1.

3.2 Validations

3.2.1 Isotropic consolidation triaxial test

Hyodo, Wu et al. (2017) carried out isotropic consolidation tests with two initial densities of dense $(e_o = 0.657)$ and medium dense $(e_o = 0.76)$ for Aio sand. As observed in Fig.(3-1b), the grading indices, I_G, derived from the relative breakage, B_r (Hyodo, Wu et al. 2017), showed small variations indicating the occurrence of slight breakage. However, the trend of denser soil exhibiting less breakage could be also observed in these tests (Fig. (3-1b)). Figs. (3-1a) and (3-1b) show that the proposed model can not only capture the stress-strain responses but also variations of grading index with different densities. In this experiment, the confining pressure was only 10 MPa which induced a slight breakage for Aio sand. However, in the following validations, confining pressures were performed to higher values to assure the occurrence of crushing.
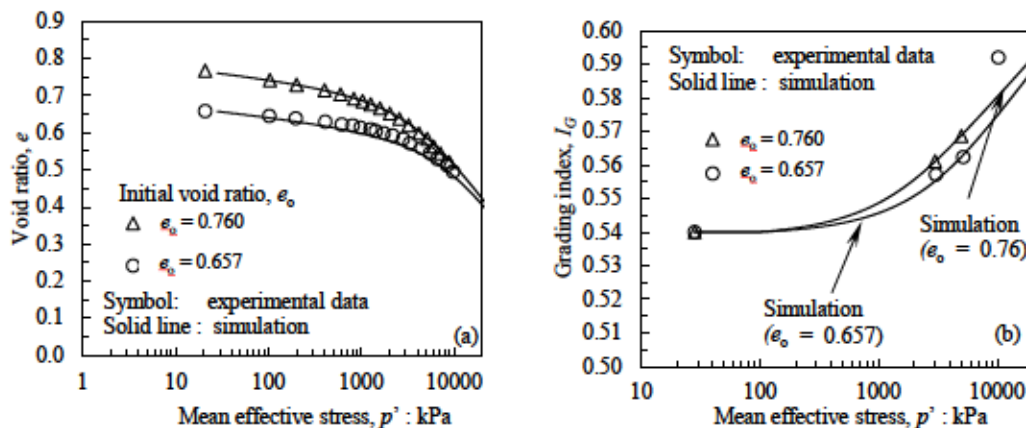
Figure 3-1: Comparison the simulation results of isotropic consolidation test and experimental results

for Aio sand by Hyodo, Wu et al. (2017): (a) compression curves; (b) variations of grading index

(derived from relative breakage , B_r) with mean effective stress.

3.2.2 1D consolidation tests

Guimaraes, Valdes et al. (2007) and Valdes (2003) presented 1D consolidation test for Ottawa sand and compressed upto a very high pressure of 100 MPa. In this test, the compression curves of dense $(e_o = 0.534)$ and loose $(e_o = 0.698)$ soils were showed in Fig. (3-2a) while, the grading indices obtained from PSD (Figs. (1-2b), (1-2c), and (1-2d)) were presented in Fig. (3-2b) for three desired pressures of 1.4MPa, 50MPa, and 100MPa. It is noted that the limit grading for Ottawa sand was obtained from the results of ring shear tests by Sadrekarimi and Olson (2010). As it was noted in the earlier section, the variations of the grading indices revealed three remarkable trends: 1) low compression pressure inducing negligible breakage; 2) Dense soils experience less breakage than the loose soil; 3) the gaps of breakage for dense soils and loose soils reduce when the compression stress increase. As observed in Figs. (3-2a) and (3-2b), the proposed model shows good performance in predicting the compression curves and capturing the overall trend of the variations of the grading indices.

Figure 3-2 show 1D compression test for Dog Bay sand (Altuhafi and Coop 2011) with three different initial densities ($e_o =1.486$, $e_o =1.672$, and $e_o =1.863$) and compressed up to 30MPa. Remarkable responses of this test were the unloading and reloading states (Fig. (3-3a)). As established from Eqs. (2-5) and (2-6)), the proposed model is capable of depicting these unloading and reloading process. Thus, the simulation results by the proposed model can capture the responses of experimental results very well (Fig. (3-3a)). Furthermore, the simulation results also confirm that the denser soils exhibited less breakage as compared to the looser soils. However, when the compressed pressure increases, the breakage of different densities approach to a asymptotical unity (Fig.(3-3a)).
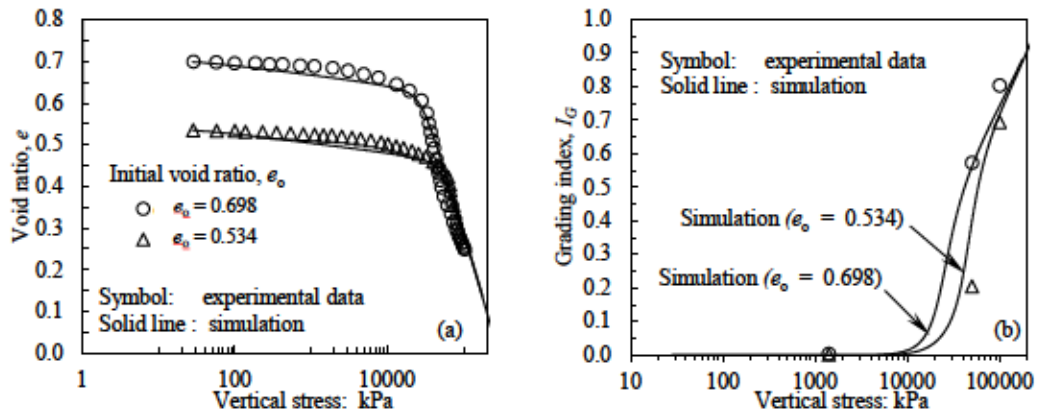
Figure 3-2: Comparison the simulation results of 1D consolidation test and the experimental results of Ottawa sand by Valdes (2003), (Guimaraes, Valdes et al. 2007):(a) compression curves; (b) variations of grading index with vertical stress.
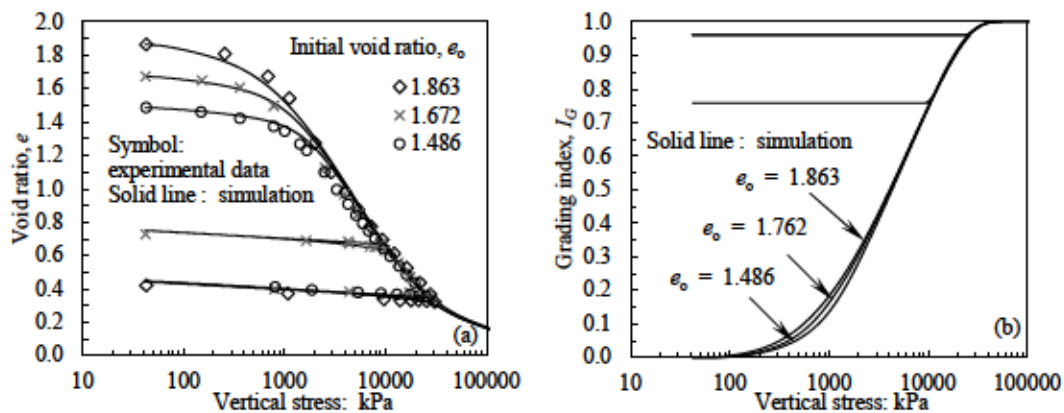
Figure 3-3: Comparisons the simulation results of 1D consolidation test for Dogs bay sand with the experimental results by Altuhafi and Coop (2011):(a) compression curves; (b) variations of grading index with vertical stress.

3.2.3 DEM simulations
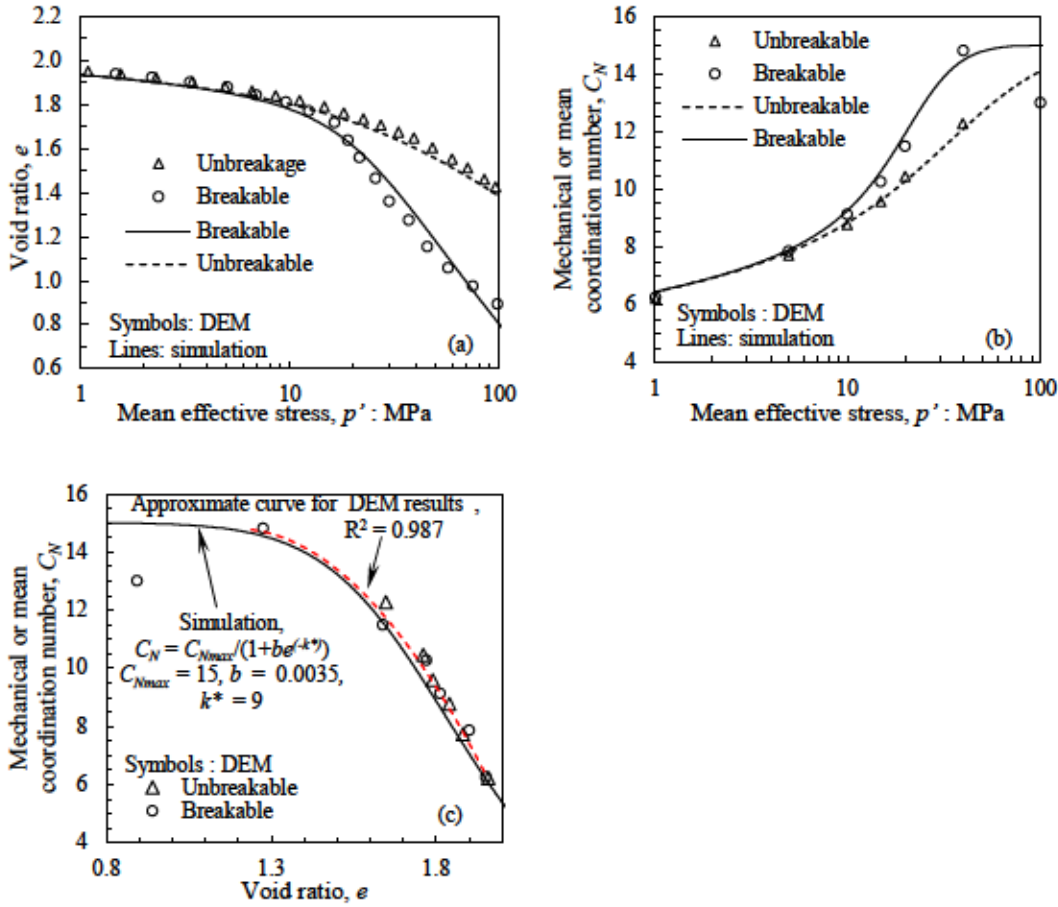
Figure 3-4: Comparisons of the results of isotropic consolidation by elementary simulation and DEM results from Bolton, Nakata et al. (2008): (a) Compression curves; (b) Variations of coordination numbers with mean effective stress; (c) Relation of coordination number and void ratio.

Bolton, Nakata et al. (2008), performed DEM simulation of isotropic consolidation for breakable and unbreakable cases. Figs (3-4a) and (3-4b) showed the results of these simulation, where the coordination number was the mechanical mean coordination number (Thornton 2000). Deriving from these DEM results, Fig. (3-4c) revealed a unique relationship between the coordination number and void ratio regardless of breakable or unbreakable simulations. Based on comparison between the simulations by the proposed model and the results of DEM (Figs. (3-4a), (3-4b), and (3-4c)), these results show very good agreement. Especially, this validation confirms the assumption of a simple relationship between the mean coordination number and density in this study.

3.2.4 Consolidated undrained triaxial tests

Next, the performances of the proposed model are verified with the consolidated undrained triaxial tests (CU) by Hyodo, Wu et al. (2017). In these tests, dense $(e_o = 0.657)$ and medium-dense $(e_o = 0.76)$ soils of Aio sand was used. These samples were initially isotropically consolidated to the desired pressure of 3000 kPa and subsequently undrained shearing was carried out. Figs.(3-5a) and (3-5b) illustrate the stress-strain relationship during the shearing state and the variations of I_G (derived from the relative breakage, B_r, in the research of Hyodo, Wu et al. (2017)) during consolidation and shearing states. As observed in Fig.(3-5b), after consolidation state, the breakage of the dense soil was less than that of the medium-dense soil. However, after shearing state, the breakage of the dense soil was higher than that of the medium-dense soil. These stress-strain and breakage responses are very well depicted by the proposed model (Figs. (3-5a) and (3-5b)).
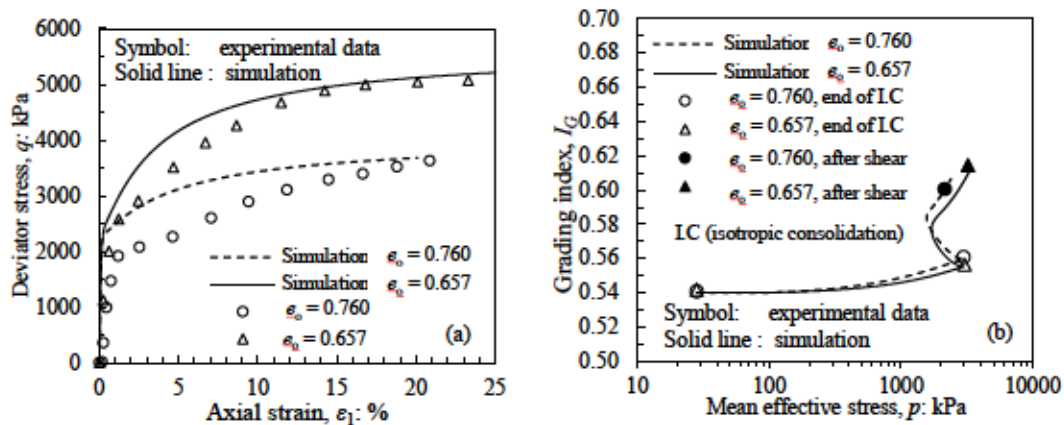
Figure 3-5: Comparisons between the results of CU test on Aio sand by Hyodo, Wu et al. (2017) and elementary simulation results using the proposed method: (a) stress-strain responses; (b) variations of grading index with mean effective stress

3.2.5 The non-uniqueness of critical state line for crushable soil under loading
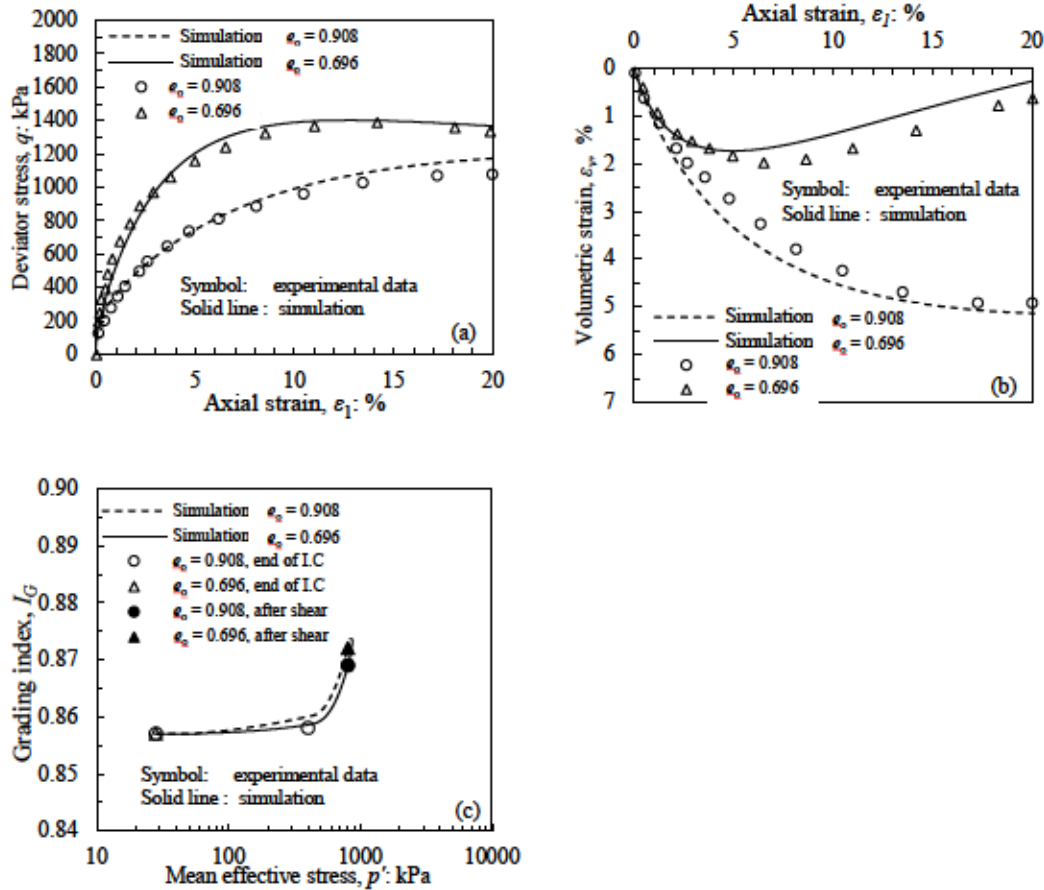
Figure 3-6: Comparisons between the results of CD test with constant radial stress for HI sand by Shahnazari and Rezvani (2013) and elementary simulation results using the proposed method: (a) stress-strain responses; (b) volumetric responses; (b) variation of grading index with mean effective stress.

Similarly, the variations of strength, volumetric contraction or dilation and grading indices in consolidated drained triaxial test (CD) with constant radial stress for HI sand performed by Shahnazari and Rezvani (2013) are verified with the simulation results by the proposed model (Figs (3-6a), (3-6b) and (3-6c)). Samples with dense $(e_o = 0.696)$ and loose $(e_o = 0.908)$ were initially consolidated isotropically up to 400 kPa and then drained shearing state was induced. Figs. (3-6a) and (3-6b) demonstrated that the proposed model can capture the trends of strength and dilatancy variations with different densities. Furthermore, it also shows that the simulation results predict the trends of variations

of grading indices very well (Fig. (3-6c)) (the denser soil exhibited more breakage than the loose soil after the shearing state).

3.3 Parametric studies

3.3.1 Breakage responses under consolidation tests

In order to investigate the response of the crushable soils under consolidation tests, a series of simulations by the proposed model with different densities for Dog Bay sand are performed. In these simulations, variations of void ratio, e, mean coordination number, C_N, and grading index, I_G, versus the mean effective stress , p', are presented in the Figs. (3-7a), (3-7b) and (3-7c), respectively. These variations are also uniquely portrayed in 3D graph (Fig. (3-7d)). In which, the grading indices depends not only on the crushing stress, p_x, but also on the variation of mean coordination number. The proposed model appropriately describes the crushing responses of crushable soil, whereas the previous model described the relationship of grading index depend only on the crushing stress.

Figs. (3-7a), (3-7b) and (3-7c) demonstrate a consistent relationship among these state parameters (void ratio, mean coordination number, and grading index) when the mean effective stress, p', increases: 1) When the mean effective stress, p', is smaller or equal to the initial crushing stress, p_{x0}, no breakage occurs. The compression curves are almost linear lines; 2) when the mean effective stress, p', higher than the initial crushing stress, p_{x0} ($p' > p_{x0}$), considerable breakage occurs. In which, the denser soils with higher coordination number, C_N, show less breakage than the looser soils. A rapid change of slopes is detected in the compression curves (Fig. (3-7a)) indicating most of plastic deformation due to particle breakage takes place; 3) when the mean effective stress, p', increases to higher confining stress, the breakage responses of the different densities show less differences, subsequently, they are unique. Correspondently, the void ratio, e, and the mean coordination number , C_N, also approach asymptotical unity. As observed in Figs (3-7a) and (3-7c), when higher confining pressure is reached, the reductions of the slopes of the compression curves are also consistent with the slowdown of the breakage rate.
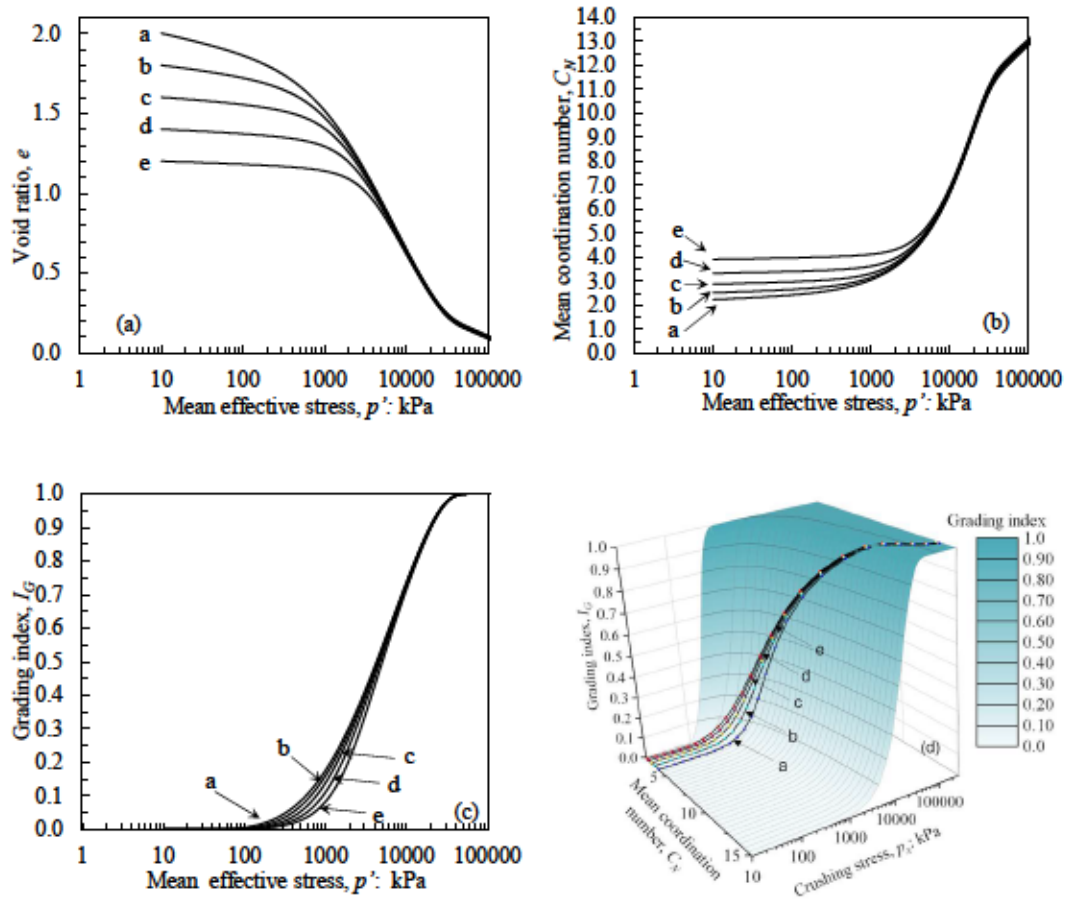
Figure 3-7: Effect of different densities under isotropic consolidation for Dogs Bay sand on the model responses: (a) compression curves; (b) variations of the mean coordination number with mean effective stress; (c) variations of the grading indices with mean effecive stress; (d) uniquely presentated the relationships of mean coordination number, crushing stress and grading index on 3D graph.

3.3.2 Contour maps presenting characteristics of the crushable soils

The 3D graph in Fig. (3-8d) is simply represented on the contour maps (Figs. (3-8a) and (3-8b) for Ottawa sand and Dogs Bay sand) of three fundamental state parameters of mean coordination number, C_N, crushing stress, p_x, and grading index, I_G. The purpose of these contour maps is to illustrate how breakage response with the effect of crushing stress, p_x, and mean coordination number, C_N. In the other words, the graphs can reveal how breakage potential of each soil and the current model can capture the characteristics. In these figures, series of simulations of isotropic consolidation with

different densities are also presented. It is noted that the denser soils have higher mean coordination number in comparison to the looser soils. Also, the isotropic consolidation lines of the denser soils reach the contour lines slower when the crushing stress, p_x, increases. The higher mean coordination number and slower reaching to the contour lines of the denser soils indicate that the denser soils can exhibit less breakage than the looser soils during isotropic compression. Figs. (3-8a) and (3-8b) also present the variations of the mean coordination number approaching to asymptotical unity when the crushing stress, p_x, increases. A remarkable characteristic of these contour maps is its reflection of deformation properties. For example, the steep slopes in the contour lines of Ottawa sand (Fig. 3-8a) indicate the brittle behavior, whereas the gentle slopes in the contour lines of Dogs Bay sand (Fig. 3-8b) indicate the ductile behavior.

Through calibration with the material parameters, the crushing potential with the effect of coordination number and crushing stress can be captures for each crushable soil by the proposed model. Therefore, the proposed model is robust and versatile for widely applications with different crushable soils.
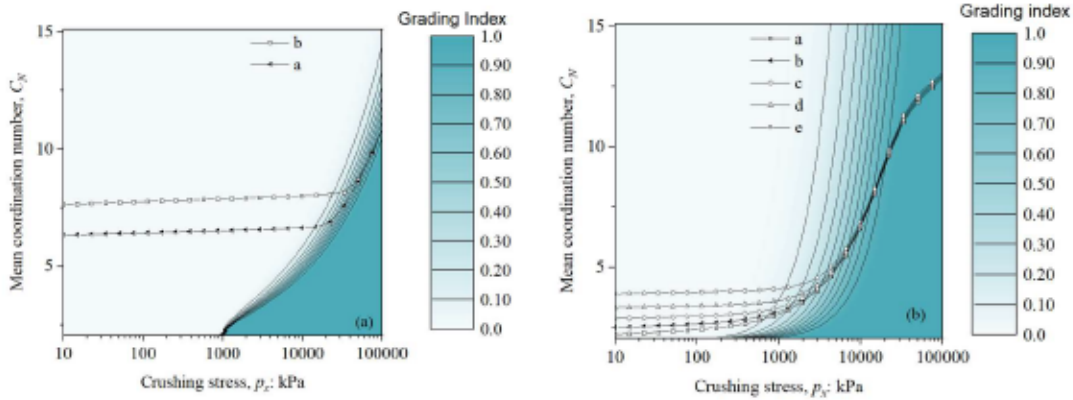
Figure 3-8: Contour maps for the relationships of mean coordination number, crushing stress and grading index: (a) Ottawa sand; (b) Dogs Bay sand.

3.2.4 Breakage responses under CU tests
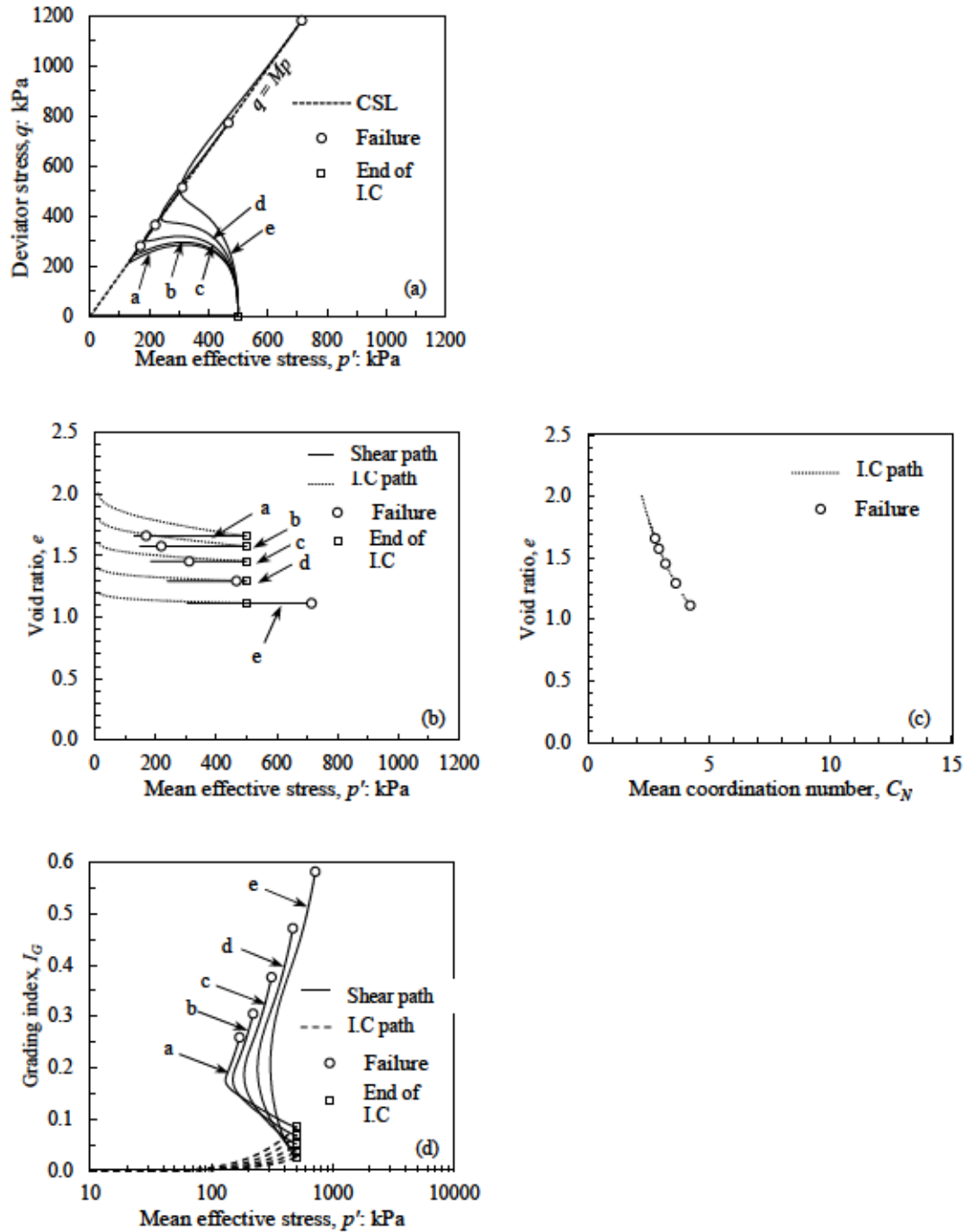
Figure 3-9: *Effect of different densities under CU tests for Dogs Bay sand on the model response: (a) p'–q plane; (b) evolution of void ratios with mean effective stress; (d) variations of grading indices with mean effective stress; (c) relationship between void ratio and coordination number.*

A series of simulations with different densities are conducted in CU tests for Dogs Bay sand shown in Figs. (3-9a), (3-9b), (3-9c), and (3-9d). The purpose of the simulations is to examine which factor that control the breakage response under CU tests. Initially, isotropic consolidations are performed to a desired confining pressure of 500 kPa followed by undrained shearing to failure. The variations of stresses, void ratio, mean coordination number, and grading index are presented in Figs (3-9a), (3-9b), (3-9c) and (3-9d). As observed in Fig. (3-9a), during consolidation state, the simulation results of the denser soils show less breakage occurrence as compared to the looser soil. However, during undrained shearing state, more breakage is presented for the denser soils. The simulation results are also consistent with experimental results by Hyodo, Wu et al. (2017). At the failure state, the simulations (Figs. (3-9a) and (3-9c)) reveal that the denser soils have higher both stresses (p',q), and the mean coordination number, C_N, as compared to the looser soils. Even though, the higher mean coordination number, C_N, may cause more resistant against breakage, but, the higher stresses (p',q) demonstrates more dominant effect of the breakage behavior at the critical state. The current model based on the interactive effect of the stresses and the mean coordination number (Eqs. (2-5), (2-6) and (2-7)) can easily capture these complex responses.

3.2.5 Breakage responses under CD tests

In order to explore the effect of initial confining pressures on particles crushing with different densities under shearing state, numerical simulations were performed for CD tests with two extreme densities of dense $(e_o = 1.2)$ and loose $(e_o = 2)$ for Dogs bay sand. Figs (3-10) and (3-11) show variations of stresses, void ratio, mean coordination number and grading index with two initially isotropically consolidated pressures of 100 kPa and 500 kPa. Several remarkable conclusions can be drawn when comparing these numerical results:

1) As observed in Figs. (3-10h) and (3-10h), the final grading indices of the dense and loose soils at the confining pressure of 100 kPa are lower than those for the confining pressure of 500 kPa. Higher confining pressure is, the more breakage exhibits. The effect of confining pressure on the

breakage response is consistent with other studies (Hardin 1985, Lade, Yamamuro et al. 1996, Shahnazari and Rezvani 2013, Hyodo, Wu et al. 2017);

2) Under low confining pressure of 100 kPa (Figs (3-10a) and (3-10g)), the dense soil is characterized with a peak strength, whereas, the loose soil has its strength increasing gradually. Similarly, as the grading index, I_G, of the dense soil reaches the maximum value, it approaches the peak strength, simultaneously. While, the grading index, I_G, of the loose soil increases gradually;

3) As observed in Figs. (3-10a), (3-10f) and (3-10h), the stresses (p',q), mean coordination number, C_N, and grading index, I_G, of the dense soil are higher than those of the loose soil. Based on the interactive effect of the stresses (p',q) and the mean coordination number, C_N, formulated in Eqs. (2-5), (2-6) and (2-7), the proposed model can easily depict the breakage phenomenon that the higher peak strength of the dense soil can overcome the resistance effect caused by the higher mean coordination number;

4) Due to different breakages encountered under low confining pressure (Fig. (3-10h)), the critical state lines (CSL) formulated from Eq. (2-17) are also not unique, demonstrated by different void ratio after shear state in Figs. (3-10c) and (3-10d);

5) Under high confining pressure of 500 kPa (Figs. (3-11a) and (3-11b)), the strengths and grading indices of the dense and loose soils gradually increase to a similar value. Also, after shearing state in Figs (3-11d) and (3-11f), void ratio and mean coordination number seem to approach to an asymptotic unity. The unique CSL can be found when high confining pressure is applied.

Figure 3-10: Effect of densities under CD tests with confining pressure 100 kPa for Dogs Bay sand: (a), (c), (e), and (g) are variations of stress, void ratio, mean coordination number, and grading index plotted with axial strain, respectively; (b), (d), (f), (h) are variations of stress, void ratio, mean coordination number, and grading index plotted with mean effective stress, respectively
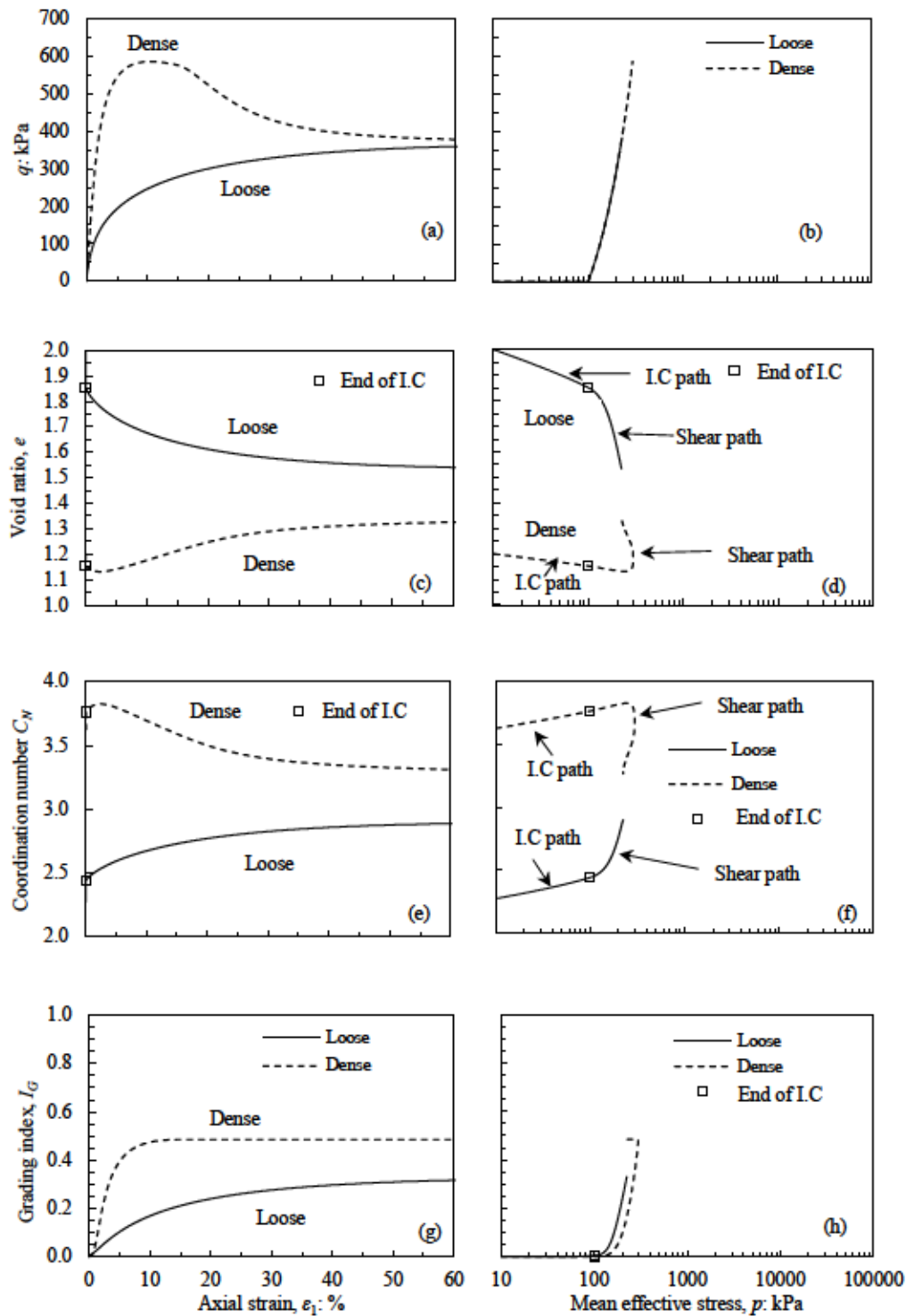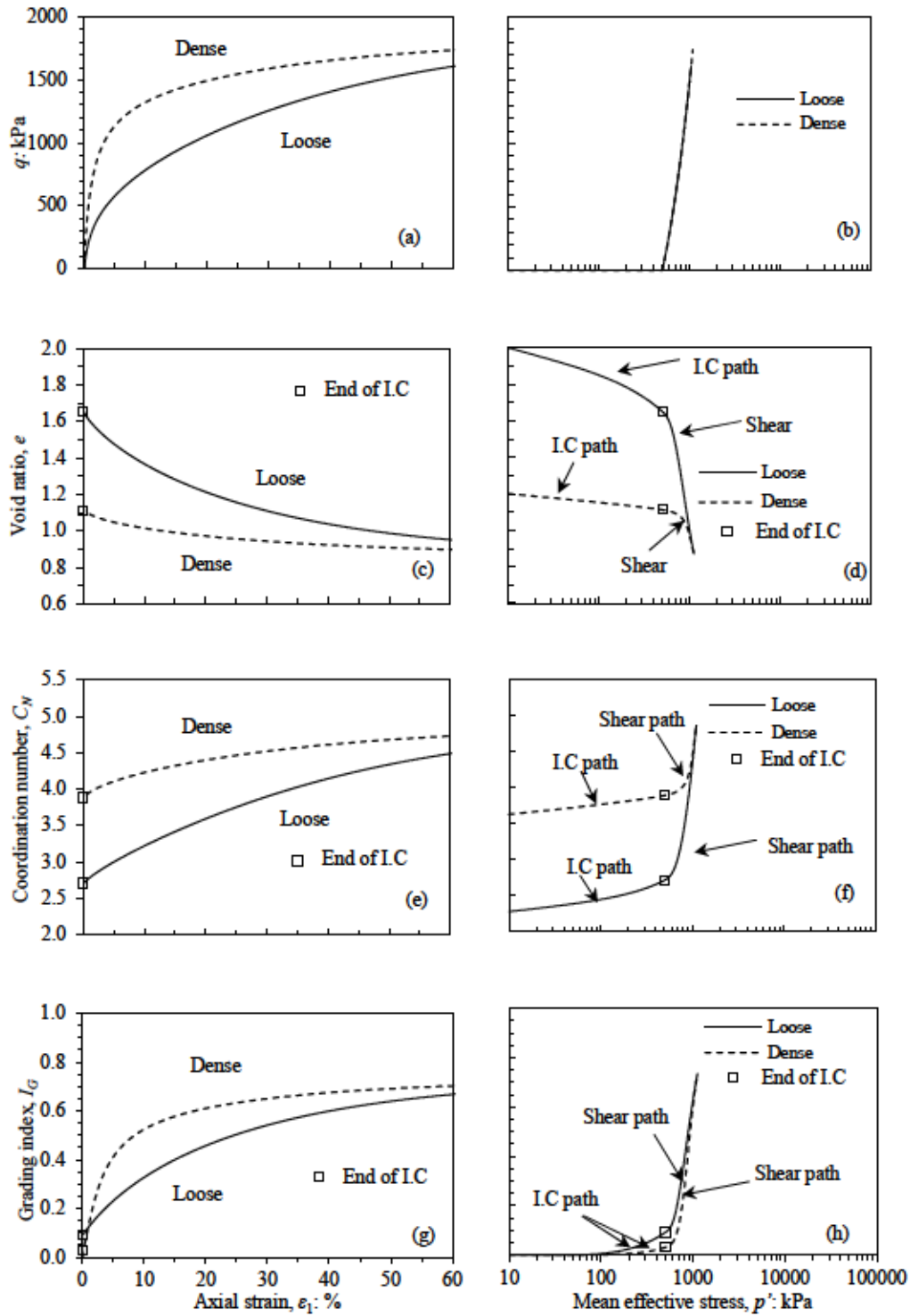
Figure 3-11: Effect of densities under CD tests with confining pressure 500 kPa for Dogs Bay sand: (a), (c), (e), and (g) are variations of stress, void ratio, mean coordination number, and grading index plotted with axial strain, respectively; (b), (d), (f), (h) are variations of stress, void ratio, mean coordination number, and grading index plotted with mean effective stress, respectively

3.2.5 Effect of density and confining pressure on the CSL

The effect of densities and confining pressures on the CSL are further examined by a series of simulation of CD test with constant mean effective stress as shown in Figs. (3-12a). In these simulations, two extreme densities for Dogs Bay sand are considered with dense $(e_o =1.2)$ and loose $(e_o = 2)$ .Samples are initially consolidated Isotropically to the desired confining pressures of 30, 50, 100, 200, 500, 1.000, 2.000, 5.000, 10.000, and 20.000 MPa, and then shearing state are performed with constant mean effective stress. After shearing state, the failure points of each tests are connected to create the CSL for dense and loose soil (Fig. 3-12a). Based on these analysis results, the CSL for the dense soil and loose soil change from non-unique to unique states when the confining pressures vary from lower to higher values, respectively. Under low confining pressure, due to the high peak strength, the dense soil exhibits more breakage than the loose soil. Thus, the CSL for the dense soil locates at lower positions as compared to the CSL for the loose soil. However, under higher confining pressures, there is no-peak strength, whereas, the coordination number tends to approach to asymptotical unity (Fig. 3-12b). Thus, the CSL for dense and loose soil are unified. This non-uniqueness was also noticed with study by (Tengattini, Das et al. 2016). However, the thermo-dynamic model by (Tengattini, Das et al. 2016) did not incorporated the coordination number, therefore, there was no clear trend of how density can effect breakage response reported.
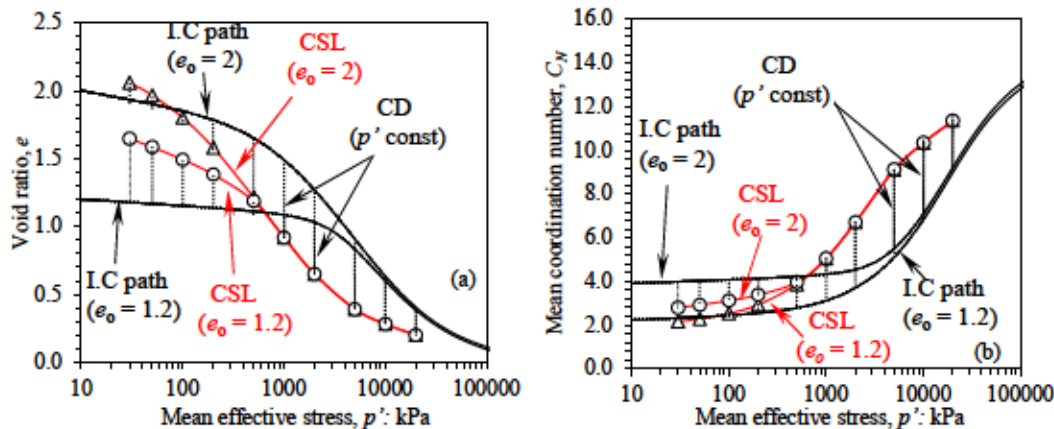
Figure 3-12: Non-uniqueness of critical state lines under different densities and different confining pressures by series of simulations of the proposed model for Dogs Bay sand: (a) on $e - \log p'$plane; (b) variations of mean coordination number at critical state.

Chapter 4 : Numerical simulation of pile's responses on crushable soils

4.1 Validation of the implementation of the proposed model into Plaxis 3D
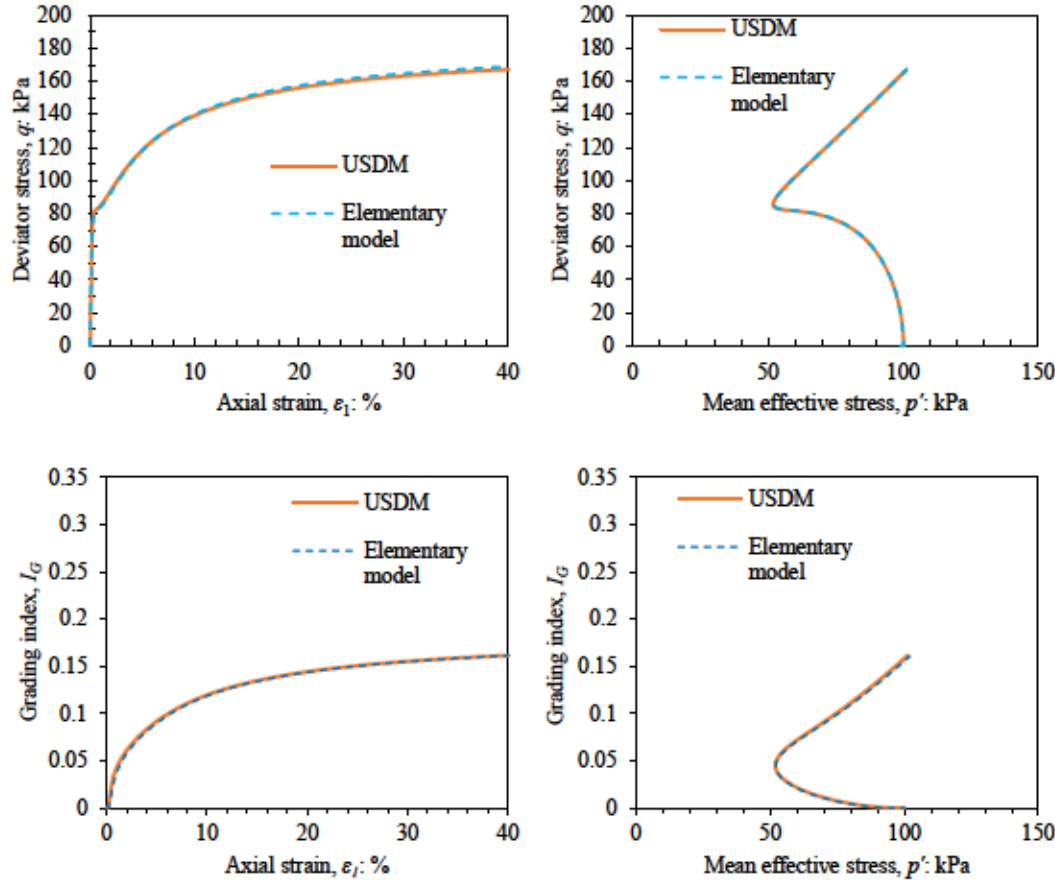
Figure 4-1: Comparison between the implemented model USDM in Plaxis and the elementary model

The bearing capacity problems of shallow and pile foundations with the Morh-Coulomb model are simulated by Plaxis and the simulation results are validated with bearing capacity formula given in The Appendix B1 and B2. These validations demonstrate the capability of Plaxis in modelling load and failure problems in geotechnical field. To study the response of pile foundation on crushable soils, the USDM of the proposed model is implemented into Plaxis. However, it is crucial to verify whether this implementation is correct or not before any further simulations of load and failure response. For

this purpose, the implementation was verified with elementary model under consolidated undrained triaxial test. In this verification, the Dog Bays sand material properties given in the table 3-1 are utilized. The initial confining pressure is 100 kPa and initial void ratio is 1.8. The Fig. 4-1 compare the variations of stress-strain and grading index between the USDM and elementary model. As can be observed from the Fig. 4-1, the results of stress-strain and grading index by both simulations of the USDM and elementary model show very well agreement. The comparisons demonstrated that the current implementation could capture the behavior of the crushable soil. Thus, the FEM model by Plaxis incorporated the USDM of the proposed model can be utilized for simulating the load and failure of single pile foundation on crushable soils.

4.2 Simulation of single pile foundation on crushable soil

In this section, the pile's responses on crushable soils are examined through FEM simulation incorporated the proposed model. Regarding the geometry for simulation, a quarter of pile model is chosen as simplification for simulation (Fig. 4-2). As can be observed in the Fig. 4-2, Pile's diameter is 1.0 m, pile's length is 10.0 m, the outer boundary with the length of 5.0m, and the soil's thickness below the pile' tip is 5m. Boundary conditions are also described in Fig. 4-2. Figure 4-3 presents the meshing model with 29635 elements of 10-node tetrahedral elements. In order to save computation time, the finer meshes are defined at the pile tip and pile shaft while, the coarser meshes are assigned at the outer boundaries.
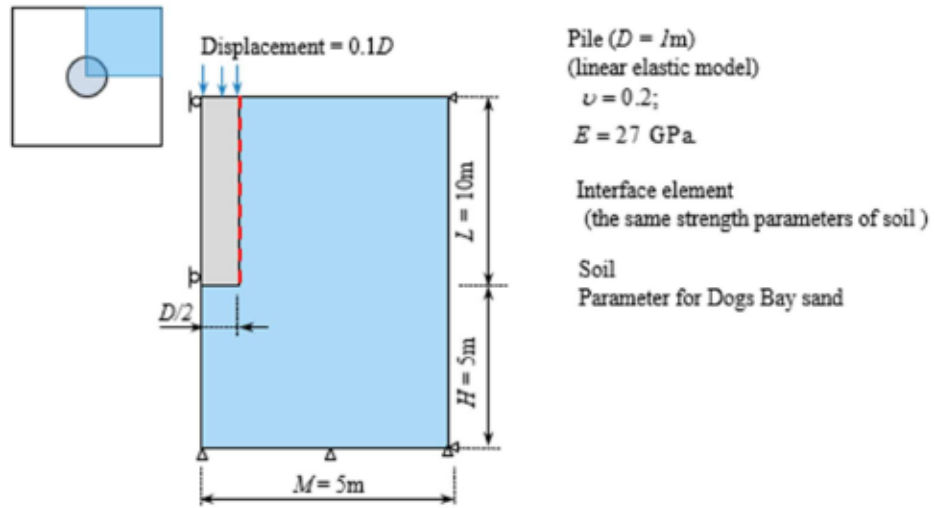
Figure 4-2: Pile's geometry
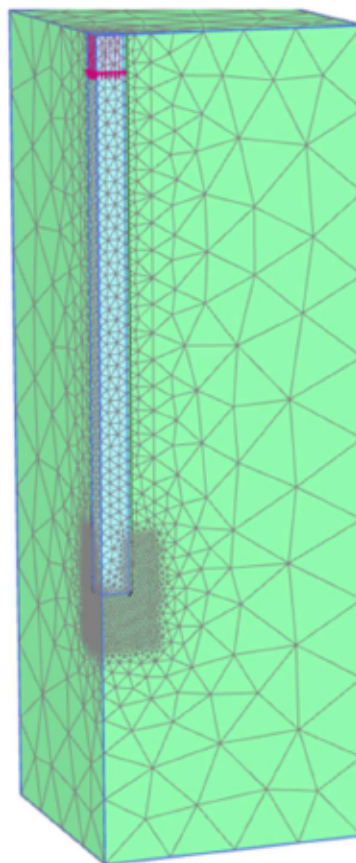
Figure 4-3: Meshing model for pile foundation

Table 4-1: Pile parameter with linear elastic model

Parameter	Description	Value	Unit
E	Young's Modulus	27	(GPa)
v_e	Poisson's ratio	0.2	

Table 4-2: Parameter for the interface's element

Parameter	Description	Value	Unit
k_s	stiffness along to the interface	10	(MPa)
k_n	stiffness normal to the interface	10	(MPa)
c_c	cohesion of interface	0	
ϕ_c	internal friction of interface	41	degree
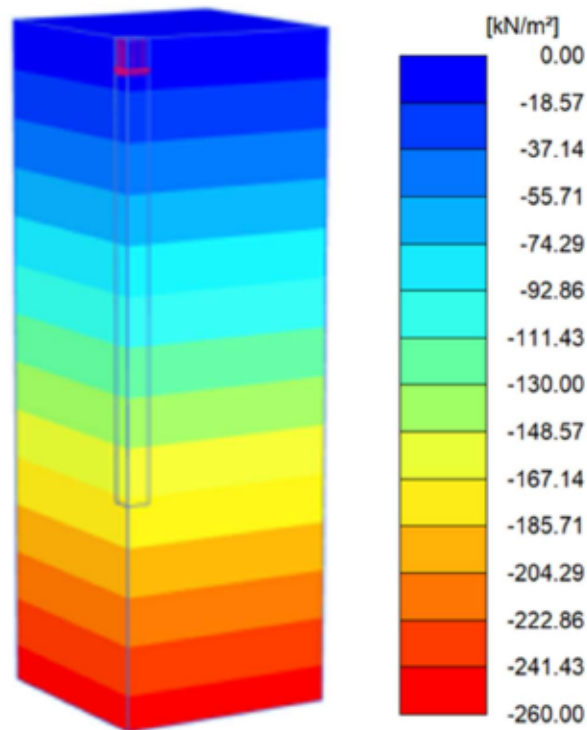
Figure 4-4: Effective vertical stress at initial state

Pile's model is simply considered as linear elastic with the parameters given in the table 4-1. As validation in the section 4.1, the USDM for Dogs Bay sand incorporated the particle crushing and the effect of packing density is utilized to examine the response of pile. The Dogs Bays sand's

parameters are given in the table 3-1. The interface properties are simply assumed with no reduction of strength. Thus, the strength of the interface element is the strength of Dogs Bay sand ($c_c = 0; \phi_c = \phi' = 41°$). The stiffness along and normal to the interface are choosen with a high value of 10 MPa for simplicity. Another assumption is no crushing happen around pile's shaft and pile's tip at the initial state. This assumption may be reasonable for piles constructed by replacement technique. While, the driven pile usually exhibit crushing around pile's tip and pile's shaft due to high concentrated stresses at the installation process. Gravity force is applied for initial state with the vertical stress distribution given in Fig. 4-4. Furthermore, displacement of 10% pile diameter ($\delta = 0.1B = 0.1m$) is defined at the pile's head. The rate of displacement is controlled by the automatic step size procedure by Van Langen and Vermeer (1990) to save computation time. In oder to study the effect of packing density on pile responses on crushable soils, two initial densities of $e_o = 2.0$ and $e_o = 1.7$ are used for the simulations.

The results of deviator strains are compared in Fig. 4-5 for the simulations with different densities ($e_o = 2.0$ and $e_o = 1.7$). In these simulations, deviator strain occurred at the pile's shaft and pile's tip. Larger magnitude of deviator strain show at the pile's tip as compared to pile's shaft. Based on the simulation results, the failure mode can be punching shear mode as the deviator strain developed around the pile's tip. Deviator strain can also be detected at the pile's head. This deviator strain at the pile's head may cause by the relative movement between the pile and soil due to the different stiffness in combination with low confining pressure at the surface.

The distributions of grading index of these simulations are compared in Fig. 4-6. As can be observed in Fig. 4-6, the distribution of grading index is more concentrated at the pile's shaft and pile's tip. Moreover, grading index distribution for the simulation of denser soil ($e_o = 1.7$) shows higher than that of the looser soil ($e_o = 2.0$). This indicates that the denser soils exhibit higher breakage as compared to the looser soil under loading of single pile.
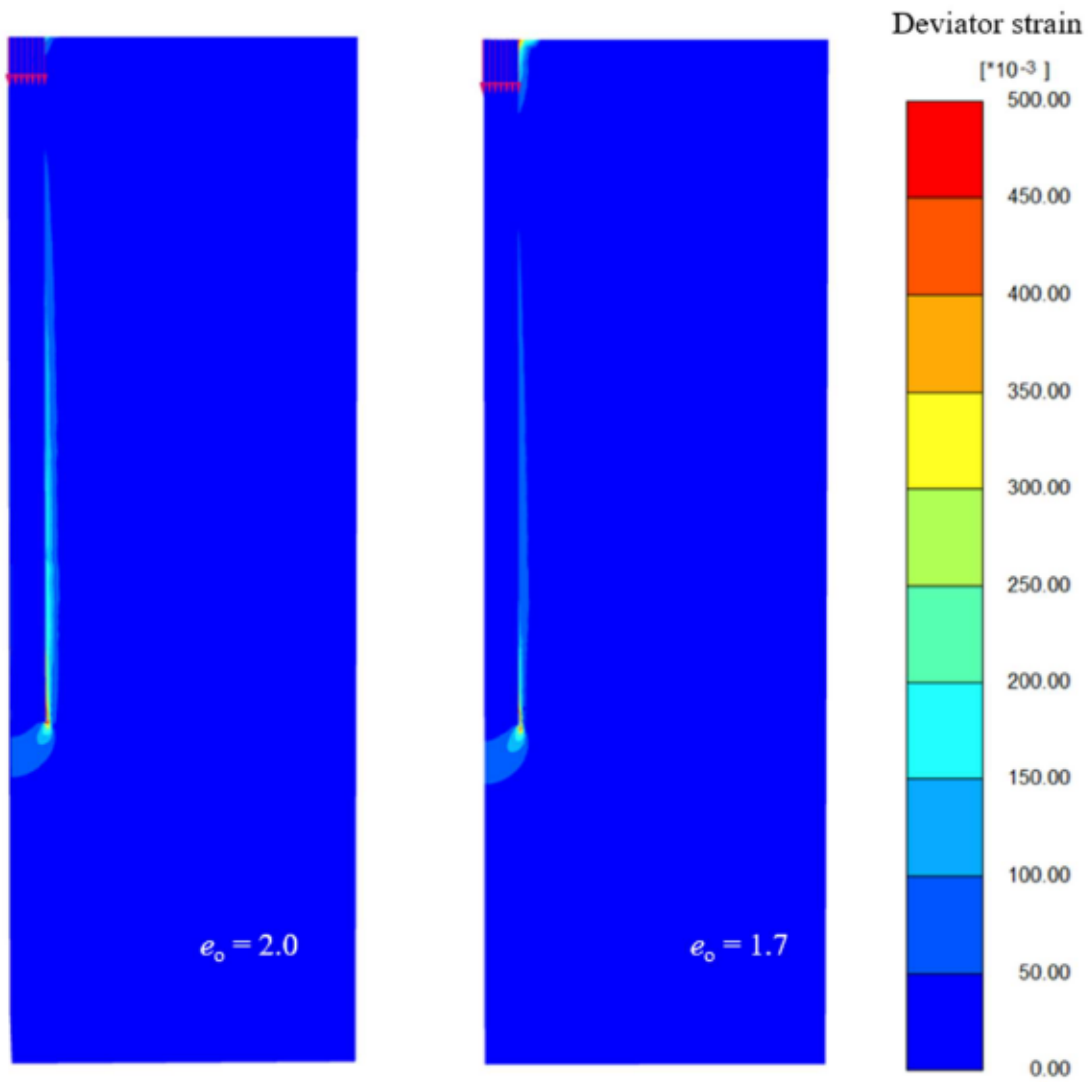
Figure 4-5: Deviator strain after simulations
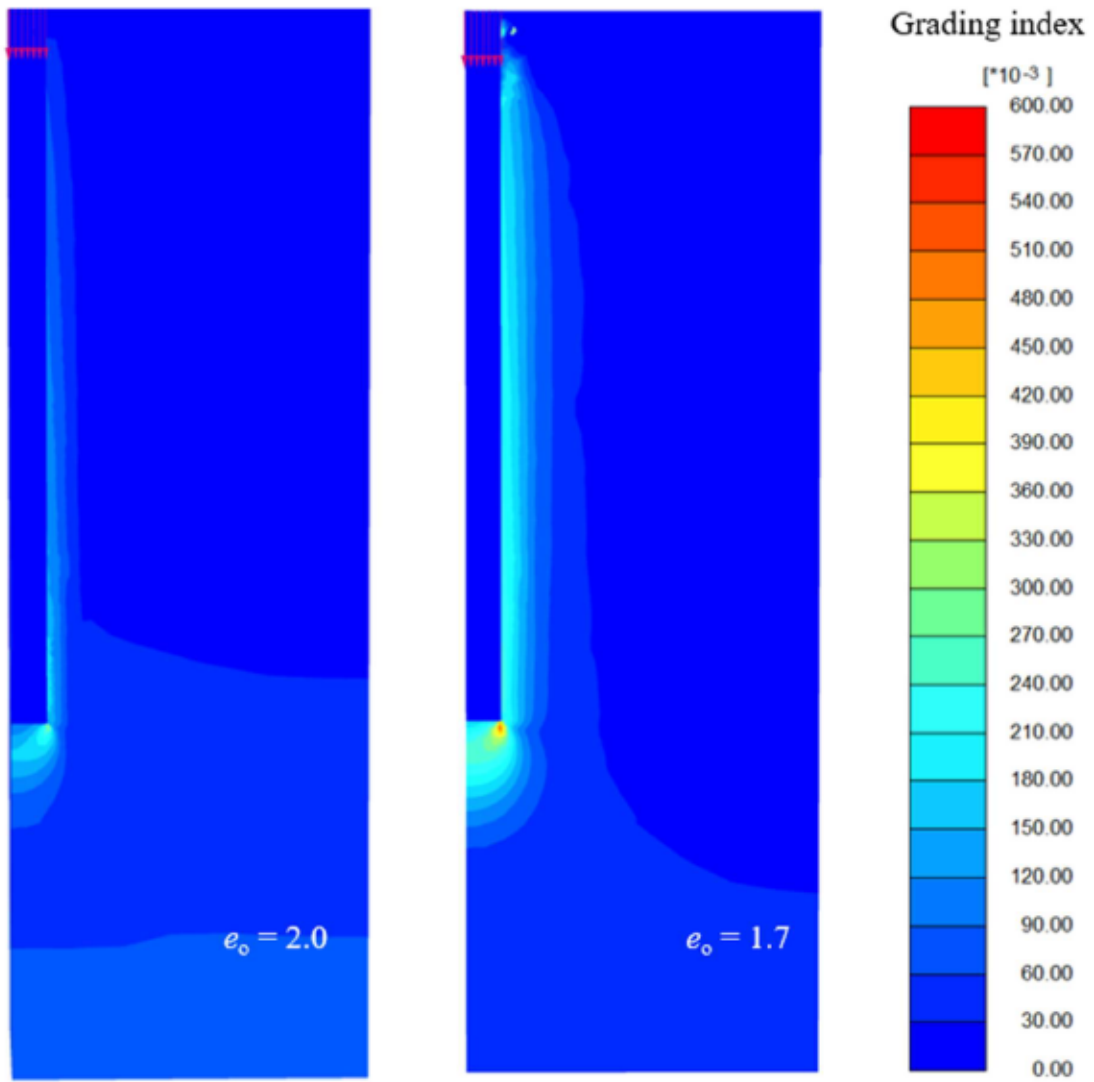
Figure 4-6: Comparison of grading index distribution
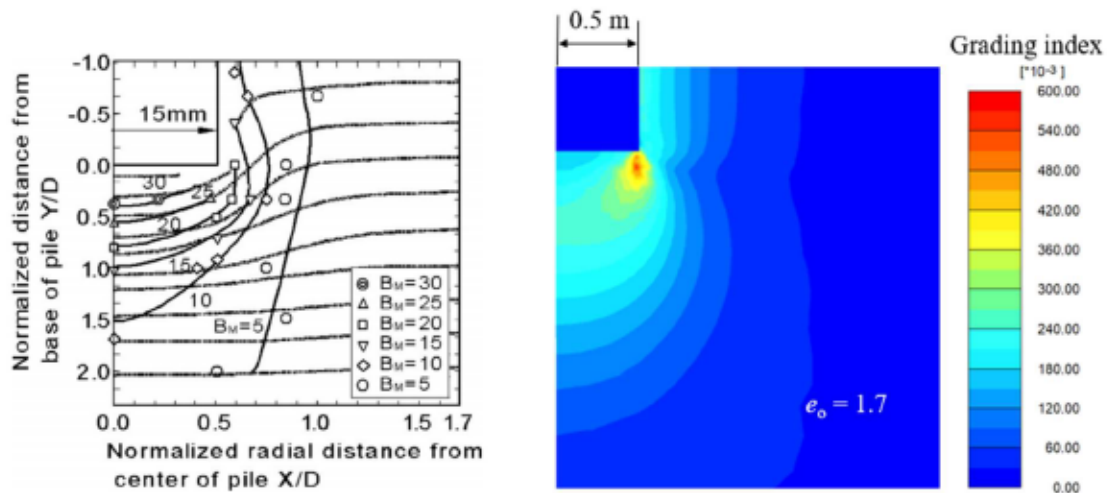
Figure 4-7: Comparison of grading index distribution at pile's tip between simulation by Kuwajima, Hyodo et al. (2009) and the simulation by the proposed model

Kuwajima, Hyodo et al. (2009), conducted a model pile load test on crushable soils and then carried out simulation for distribution of breakage factor. The comparison between the results of simulation by Kuwajima, Hyodo et al. (2009) and the simulation by the proposed model are shown in Fig. 4-7. Similar patterns of contour lines at the pile's tip and pile shaft are observed for both simulations. However, the simulation results by the proposed model show more breakage occurred at the pile's tip conner. This region with high concentrated of deviator stress and mean effective stress may cause extreme particle crushing.
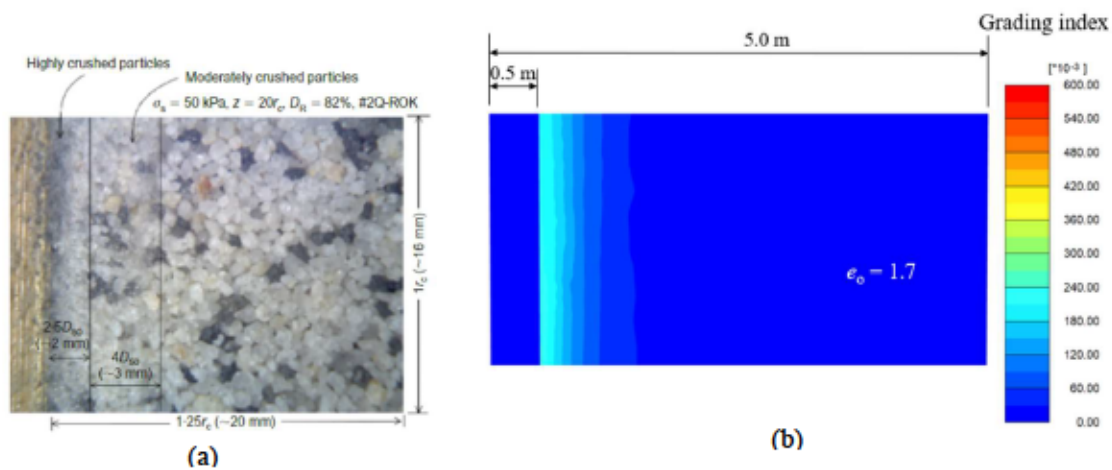
Figure 4-8: Breakage resoponses in the region adjacent to the pile shaft; a) close view image (Arshad, Tehrani et al. 2014); b) simulation results by the proposed method
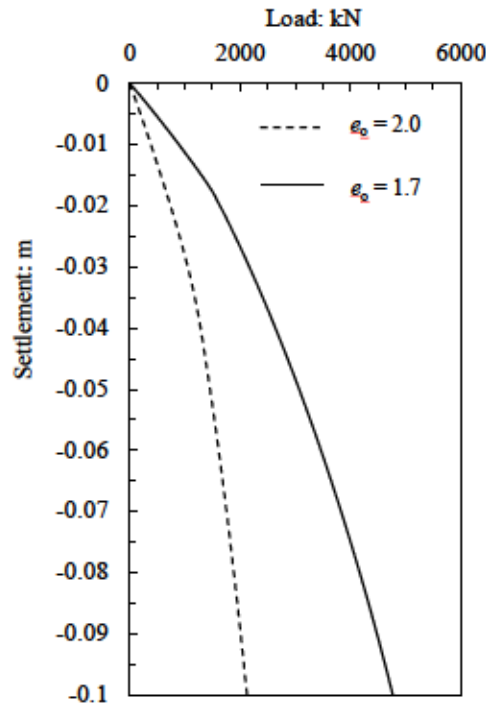
Figure 4-9: Load and settlement of simulations by the proposed model.

Arshad, Tehrani et al. (2014), performed cone penetration on an angular silica sand and a close view image of broken particle around the cone's shaft was shown in the Fig. 4-8 (a). As can be observed, the adjacent region around cone's shaft can be divided into three zones: Highly crushed particles, moderately crushed particles, and non-crush zone. Similarly, the simulation's result by the proposed model also shows the exist of particle crushing zone adjacent to the pile shaft (Fig. 4-8 (b)). The breakage reduces sharply with the distance from the pile's shaft.

The load and settlement curves by the simulations with different densities are presented in Fig. 4-9. As can be seen from the Fig. 4-9, ultimate load cannot be detected and the load increase with the increase of settlement. The reason for that may come from the failure mode is punching shear. The simulation of the denser soil ($e_o = 1.7$) shows higher load as compared to the simulation's results of the looser soil ($e_o = 2.0$). This simulations results are also consitant with the experimental results of pile load tests on Dog Bays sand by Yasufuku and Hyde (1995) (Fig.1-10).

4.3 Discussions of the simulation's results under the effect of density

4.3.1 Stress induce crushing of the elements under pile' tip

The purpose of this section to examine how stress induce crushing of the elements under pile's tip with the effect of density. This section is necessary because it can help to explain the how crushing responses under pile tip also explain the mechanics of load transfer from pile to the surrounding soil. As can be observed from the Fig. 4-7 of the grading index distribution beneath the pile's tip, the breakage occurred non-uniformly and concentrated highly at the pile conner. The other results of deviator stress, mean effective stress, volumetric strain and deviator strain also reveal that the concentrated of stress and strain is a zone starting from the pile conner and spreading to the 0.5D under pile tip (Fig. 4-10). Based on the distribution of the deviator strain, it can be assumed of a shear band formation stretched from the pile conner to 0.5D under pile tip. A long the assumed shear band, higher deviator stress is detected. Therefore, it is also reasonable explanation of the higher breakage occur. In order to understand the crushing responses under the pile's tip, 4 elements inside and outside the assumed shear band are selected as showed in the Fig. 4-11: Element A locates at the pile's center and right below the pile's tip; Element B stays at the pile conner; Element C locates at the pile's center and 0.5D from the pile's tip; Element D stays at 1.0D from the pile's tip. Among these elements, elements B and C are inside the assumed shear band, whereas elements A and D are outside the assumed shear band.

As can be observed in the Fig. 4-12, element B experiences highest deviator stress and mean effective stress, therefore, the highest breakage can be detected in the element B. In comparison between elements A and C, one may expect more crushing occur in the element A because it locates closer to the pile's tip. However, based on the simulation results in Fig.4-12 (b), the element C exhibits more crushing than element A. The stress path in Fig. 4-12 (a) revealed that element C experiences higher deviator stress than element A. Therefore, the deviator stress may dominate the crushing response and lead to more crushing for element C. Finally, element D locates far from the pile's tip and experience lowest stress. Therefore, it can be easily to understand the least crushing occur in the element D (Fig. 4-12). The stress inducing crushing of the elements revealed that the elements along the assumed shear band exhibit high crushing due to the higher deviator stress.

Similarity, the stress paths, and distribution of grading indices for the simulations with loose soil (eo = 2.0) are shown in the Figs.4-13 (a) and (b), respectively. As observed from the Figs. 4-13, Even though, the stress paths and distribution of grading indices of the simulations with loose soil show similar patterns, the smaller values of stress and grading indices after the tests can be seen. Therefore, In simulations with the loose soil, elements exhibit similar stress path but lower value, followed by

smaller values of breakage as compared to the results of the elements when simulated with the dense soil.

In order to compare the stress path and breakage of the elements under pile's tip with different densities, The stress path of each element are compared in Fig. 4-14 and the variations of grading indices are compared in Fig. 4-15. It can be seen from the Fig. 4-14, the stress paths of the elements are almost similar apart from elements C and D with a slightly differences. Moreover, the variations of grading indices can be observed in Fig. 4-15 that the loose soil always higher with the same mean effective stress. The experimental evidence also demonstrated that the loose soil experienced more breakage as compared to the dense soil under the same stress path due to their lower mean coordination number. Therefore, the crushing responses under pile foundation structure with the effect of density can be reasonably captured by the proposed model.
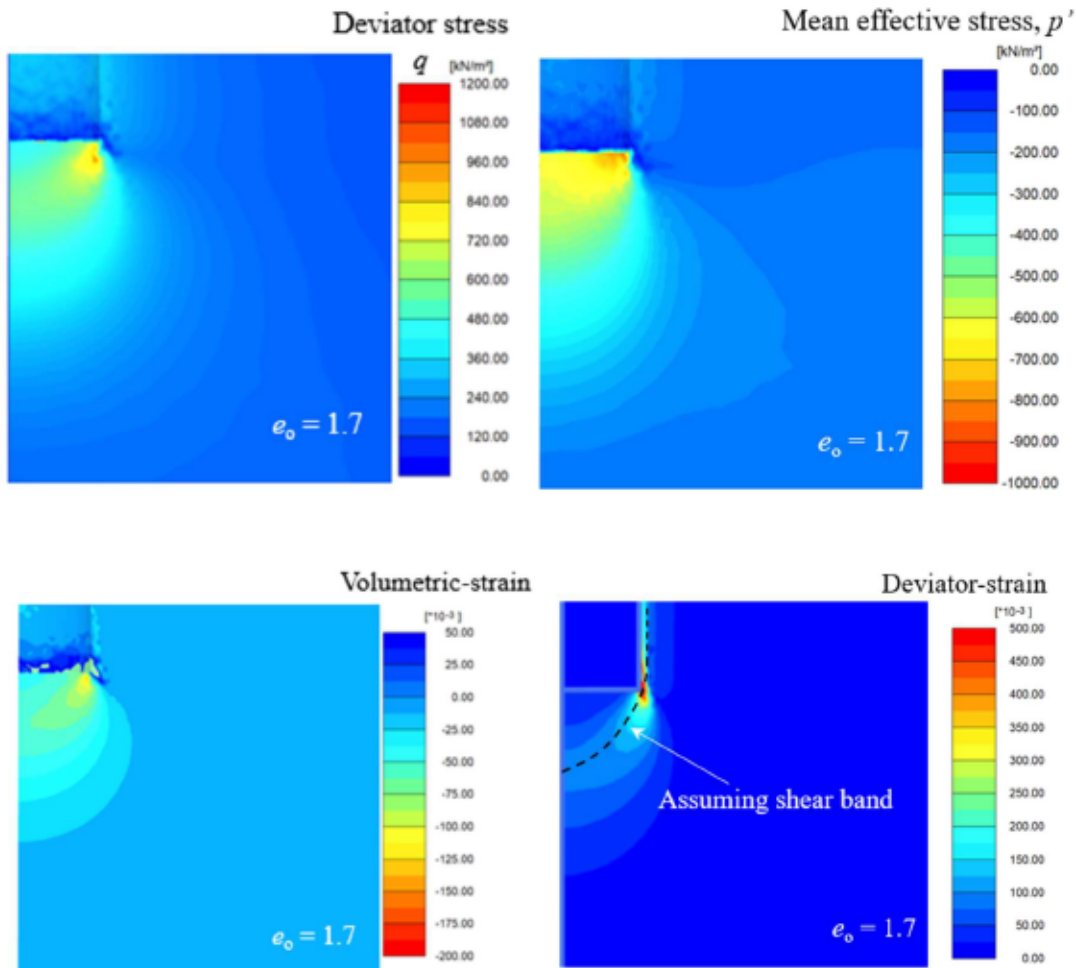
Figure 4-10: Stress and strain under pile's tip for the simulation with dense soil $e_o = 1.7$
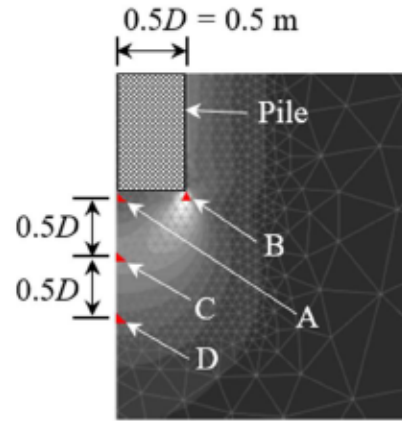
Figure 4-11: selected elements under pile's tip
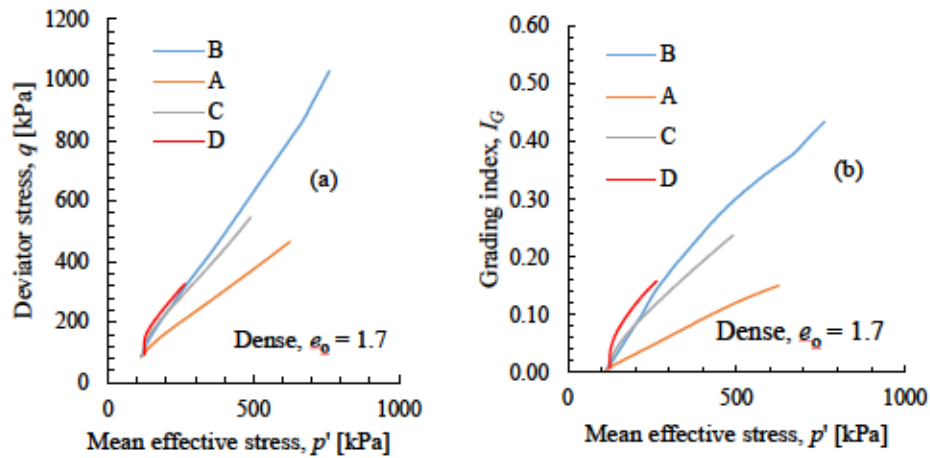
Figure 4-12: The simulation with dense soil e_0 =1.7: (a) Stress paths of the elements under pile's tip; (b) variations of grading index of the elements under pile's tip
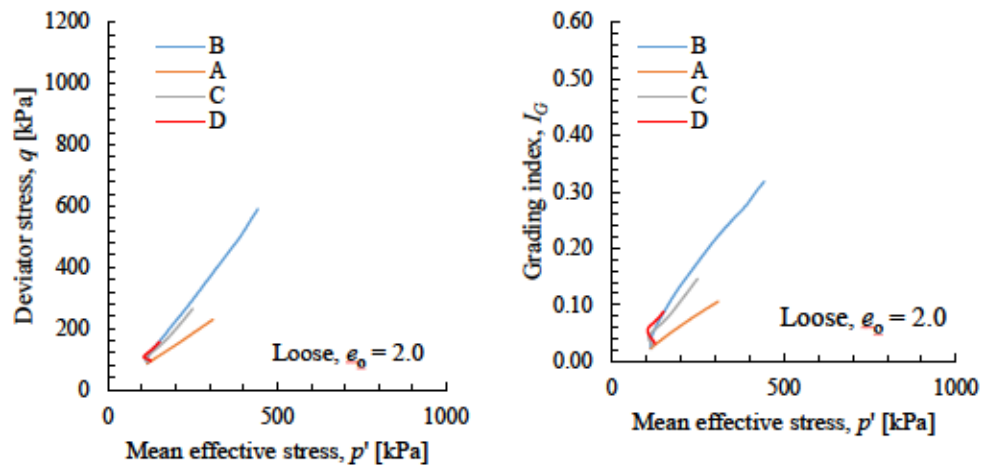
Figure 4-13: The simulation with loose soil $e_0 = 2.0$: (a) Stress paths of the elements under
pile's tip; (b) variations of grading index of the elements under pile's tip
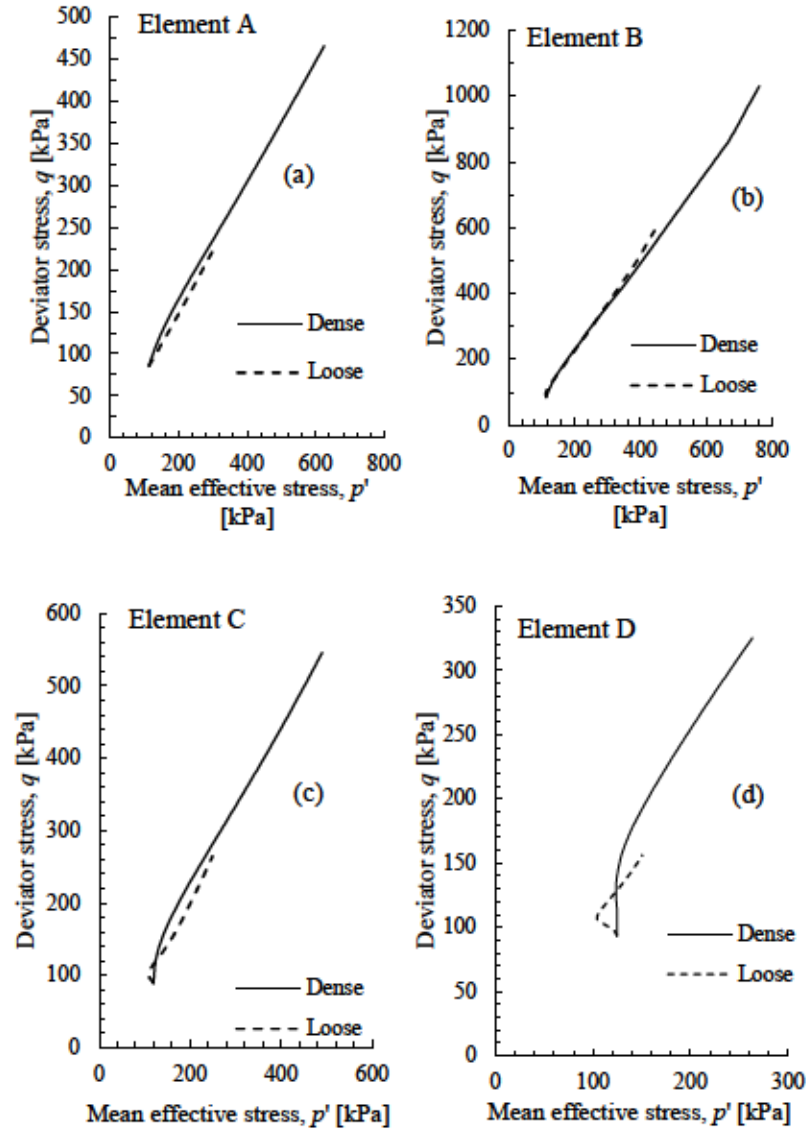
Figure 4-14: Comparison the stress paths of the simulations of the loose and dense soil: (a)
element A; (b) element B; (c) element C; (d) element D.
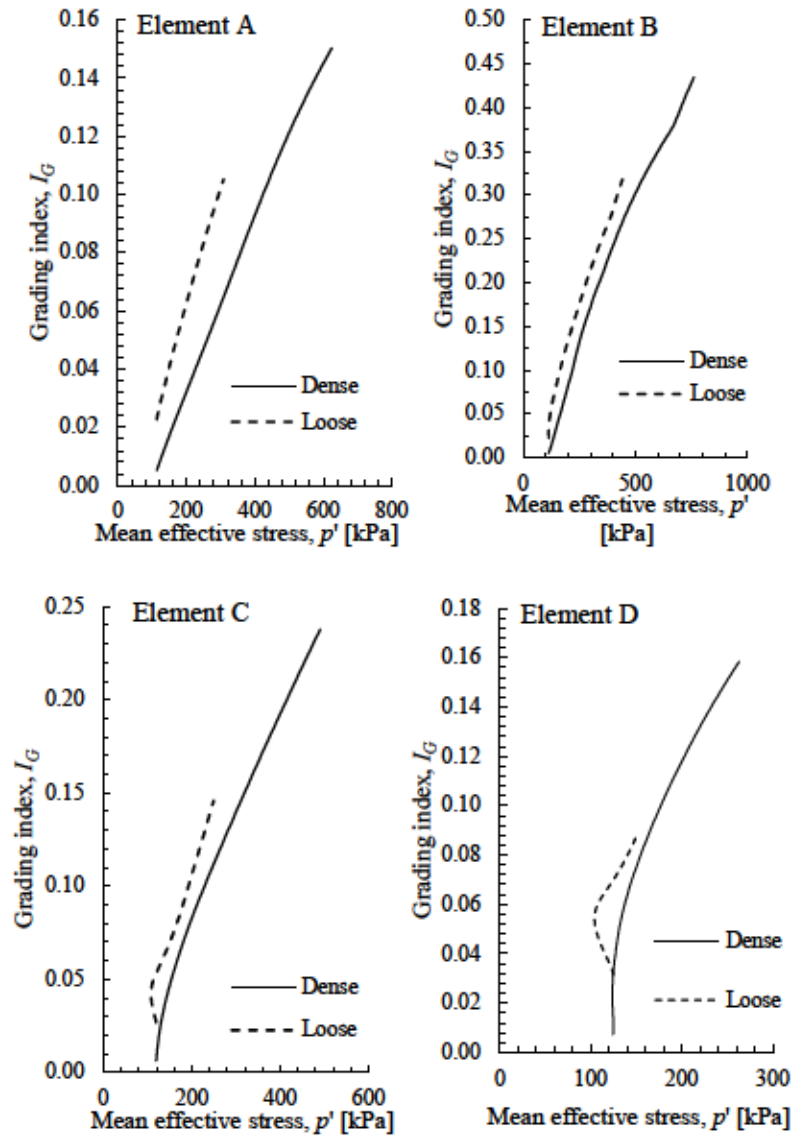
Figure 4-15: Comparison the grading index with mean effective tress of the simulations of the loose and dense soil: (a) element A; (b) element B; (c) element C; (d) element D.

4.3.2 Effect of crushing between crushable and uncrushable simulation

To examine the effect of particle crushing on the load-settlement curve, the simulations with crushable and uncrushable soil were performed for the soil with different desities of loose ($e_o = 2.0$) and dense ($e_o = 1.7$) (Figs. 4-16 a and b). As can be observed from Fig. 4-9 (a and b), particle crushing cause reduction of resistance for pile for both simulation results of the loose and dense cases. However, the load variations between the crushable and uncrushable simulations in the case of loose soil reveals a gradual increase, while the load variations in the case of dense soil escalate significantly when the settlement rising over 0.02m. Overall, dense soil experiment more reduction in bearing resistance due to more crushing occurring for the simulation with the dense soil.
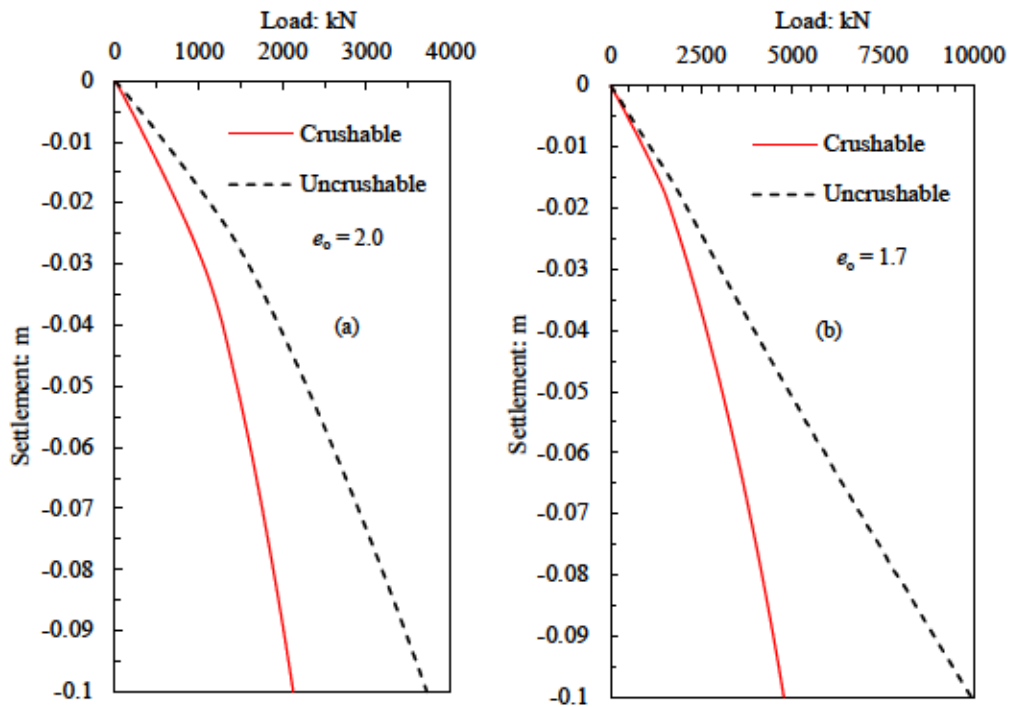
Figure 4-16: Load settlement curves for crushable and uncrushable simulations: (a) loose soil $e_o = 2.0$; (b) dense soil $e_o = 1.7$

4.3.3 Effect density on bearing resistance

In order to examine the effect of density on bearing resistance the results of physical model tests on Dogs Bay sand by Yasufuku et al. (1995) was ultilized and shown in the Fig. 4-17 (a). In Fig. 4-17(a), the resistance of pile increased when the relative density increase from 40% to 90%. However, in the physical model, the author performed the tests with steel pile which cause much less friction angle at the interface layer. The friction angle between the steel plate and soil was examined by Tanaka et al. (1995) through direct shear tests. Figs 4-17 and 4-18 illustrated the shearing resistance at the interface layer with different normal stress for Chibishi sand and Dogs Bay sand. The final results of firction angle at the interface layer can be summarized in the Fig. 4-19. As observed from the Fig. 4-19, The friction angle of Chibishi and and Dogs bay sand reduced and reached to stable state when normal stress increased. Also, the average friction angle for the interface layer of Dogs bay sand can be 8 degree. Therefore, the current simulations are updated with the interface friction angle of 8 degree and the simulation results are presented in Fig. 4-20. The experiemental results by Yasufuku et al 1995 and the simulation results shown good agreement indicated that the proposed model can capture the effect of density.
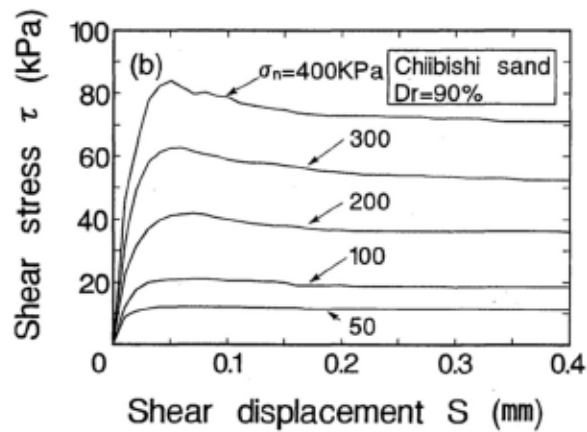
Figure 4-17: Behaviour of friction between stainless steel plate and Chibishi sand (Tanaka et al . 1995)

Figure 4-18: Behaviour of friction between stainless steel plate and Dogs Bay sand (Tanaka et al . 1995)

Figure 4-19: Comparison of angle of interface friction (Tanaka et al . 1995)
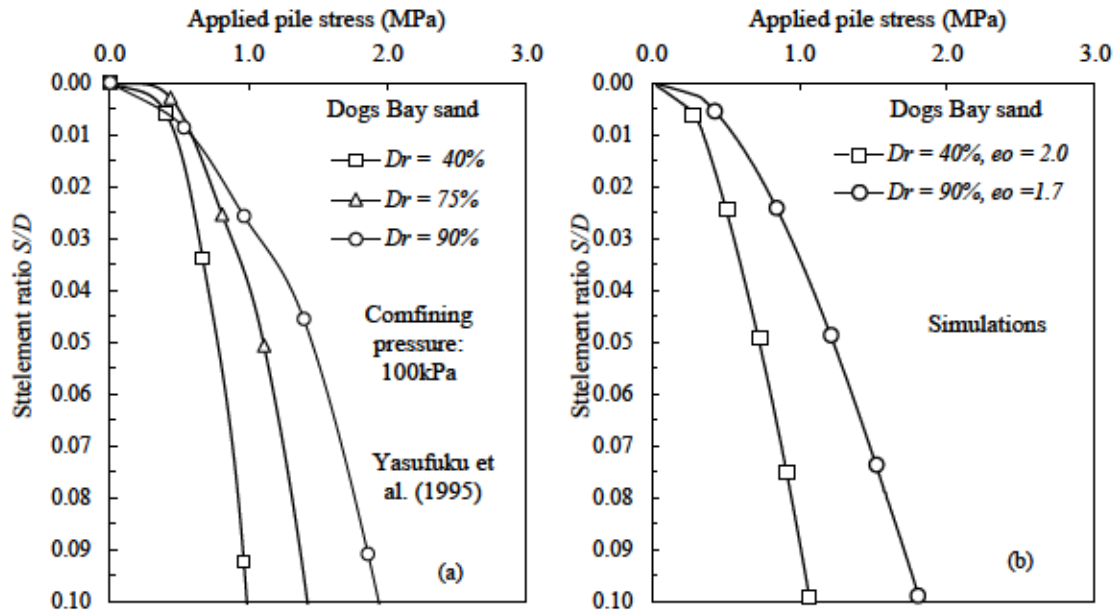
Figure 4-20: (a) Physical model tests by Yasufuku et al. 1995; (b) simulation results

Chapter 5 : Conclusions

5.1 Conclusions

In this study, a constitutive model for crushable soil incorporated the effect of packing density on the particle crushing phenomena through coordination number is establish. By examining the systematic packings and experimental packing results, a ge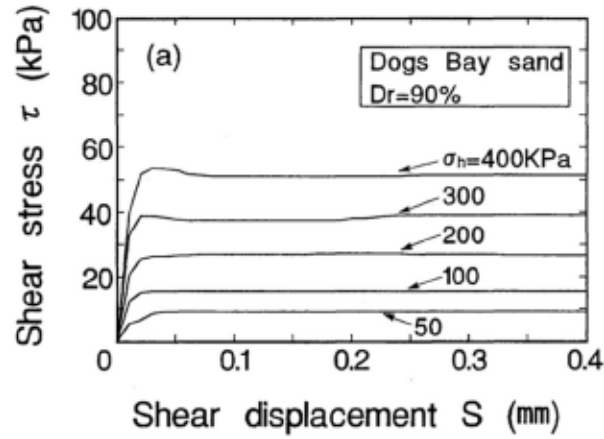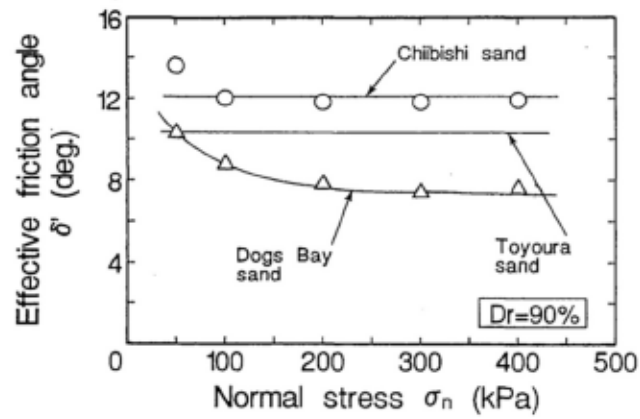neral relationship between the packing density and mean coordination number is proposed. A rational evolution rule for grading index considering the continuity of packing density and crushing resistance relationship (such as increase of density as increase of resistance against crushing due to the increase of coordination number) is established. Subsequently, the evolution rule for grading index is incorporated into the proposed constitutive model which takes account of crushing effect by lowing the critical state specific volume with the changing grading due to crushing. The validity of the proposed model is verified by comparing the simulation results with an extensive series of elementary tests. Based on the parametric studies by the proposed model for crushable soils, several findings can be listed as:

1) under the same effective stress path (such as isotropic consolidation or 1D consolidation), the model responses reveal that the densely packed soils with higher mean coordination number have lesser crushing as compared to the loosely packed soils. However, the grading index, density, and mean coordination numbers approach to an asymptotical unity when the confining stress increases;

2) Under undrained shear path, the denser soil present higher breakage. The higher deviator stress may overcome the resistance of high mean coordination number in densely packed soils and lead to more likely crush than the loosely packed one;

3) Under drained shear path, the model responses with different densities reveal significant effect by the magnitude of the initial confining pressure. When the initial confining pressure is low, the dense soil shows the high peak strength. The high peak strength may have stronger effect than the resistance caused by high coordination number of the densely packed soils. Thus, the dense soil may exhibit more breakage than the loose soil. When the initial confining pressure is high, no peak strength

is detected. In this state, the stress paths of loosely packed soils and densely packed soil is almost the same. Thus, the void ratio, coordination number, stresses, and grading index may approach to an asymptotical unity;

4) The CSL with different densities are also significantly affected by the confining pressures. The non-uniqueness is detected when the confining pressure is low. The high peak strength for denser soils is the main factor responsible for non-uniqueness at this state. However, when the confining pressure is high, the SCL approaches the same curve.

Numerical simulation of single pile foundation on crushable soils can capture the breakage responses under different densities. There are several findings from the simulations can be summarized as:

1) The failure mode of pile foundation on the crushable soils can be the punching shear mode;

2) More breakage concentrates at the pile tip and pile shaft which are consistent with experimental results;

3) Under pile's tip, along the assumed shear band, more breakage occurs due to higher deviator stress. Similar stress path can be found at the elements for simulations of loose and dense cases. However, the dense case revealed larger in the magnitude of stress in the elements leading to more crushing after simulation. Comparison of the results of grading indices in the elements shows that the grading index of the loose case always higher than the dense case when they have the same mean effective stress;

4) Preliminary results show that denser soils exhibited more breakage and experience more reduction of bearing resistance;

5) More resistance for the simulation of pile on crushable soil with dense soil as compared to the loose soil.

5.2 Future research

In the future research, further study of numerical simulation on crushable soils by the proposed model including:

1) Study the end bearing capacity under the effect of density

2) Study the skin resistance under the effect of density.

3) Propose a bearing capacity equation for pile foundation based on simulation results

REFERENCES

Aïm, R. B. and P. le Goff (1968). "La coordinance des empilements désordonnés de sphères. Application aux mélanges binaires de sphères." Powder Technology 2(1): 1-12.

Altuhafi, F. N. and M. R. Coop (2011). "Changes to particle characteristics associated with the compression of sands." Géotechnique 61(6): 459-471.

Angemeer, J., et al. (1975). Pile load tests in calcareous soils conducted in 400 feet of water from a semi-submersible exploration rig. Offshore Technology Conference, OnePetro.

Arshad, M. I., et al. (2014). "Experimental study of cone penetration in silica sand using digital image correlation." Géotechnique 64(7): 551-569.

Bandini, V. and M. R. Coop (2011). "The Influence of Particle Breakage on the Location of the Critical State Line of Sands." Soils and Foundations 51(4): 591-600.

Been, K. and M. G. Jefferies (1985). "A state parameter for sands." Géotechnique 35(2): 99-112.

Beresford, R. H. (1969). "Statistical Geometry of Random Heaps of Equal Hard Spheres." Nature 224(5219): 550-553.

Bolton, M. D., et al. (2008). "Micro- and macro-mechanical behaviour of DEM crushable materials." Géotechnique 58(6): 471-480.

Bouvard, D. and F. F. Lange (1991). "Relation between percolation and particle coordination in binary powder mixtures." Acta Metallurgica et Materialia 39(12): 3083-3090.

Coop, M. R. (1990). "The mechanics of uncemented carbonate sands." Géotechnique 40(4): 607-626.

Daouadji, A., et al. (2001). "An elastoplastic model for granular materials taking into account grain breakage." European Journal of Mechanics - A/Solids 20(1): 113-137.

Dutt, R. and A. Cheng (1984). Frictional response of piles in calcareous deposits. Offshore Technology Conference, OnePetro.

Einav, I. (2007). "Breakage mechanics—Part I: Theory." Journal of the Mechanics and Physics of Solids 55(6): 1274-1297.

Einav, I. (2007). "Breakage mechanics—Part II: Modelling granular materials." Journal of the Mechanics and Physics of Solids 55(6): 1298-1320.

Gajo, A. and D. Muir Wood (1999). "A kinematic hardening constitutive model for sands: the multiaxial formulation." International Journal for Numerical and Analytical Methods in Geomechanics 23(9): 925-965.

Gajo, A. and D. Muir Wood (1999). "Severn–Trent sand: a kinematic-hardening constitutive model: the q–p formulation." Géotechnique 49(5): 595-614.

German, R. M. (1989). "Particle packing characteristics."

German, R. M. (2014). "Coordination number changes during powder densification." Powder Technology 253: 368-376.

German, R. M. and Z. A. Munir (1975). "Morphology relations during surface-transport controlled sintering." Metallurgical Transactions B 6(2): 289-294.

Ghafghazi, M., et al. (2014). "Particle breakage and the critical state of sand." Soils and Foundations 54(3): 451-461.

Goodman, R. E., et al. (1968). "A Model for the Mechanics of Jointed Rock." Journal of the Soil Mechanics and Foundations Division 94(3): 637-659.

Graton, L. C. and H. J. Fraser (1935). "Systematic Packing of Spheres: With Particular Relation to Porosity and Permeability." The Journal of Geology 43(8, Part 1): 785-909.

Guimaraes, M. S., et al. (2007). "Aggregate production: Fines generation during rock crushing." International Journal of Mineral Processing 81(4): 237-247.

Hardin, B. O. (1985). "Crushing of Soil Particles." Journal of Geotechnical Engineering 111(10): 1177-1192.

Haughey, D. P. and G. S. G. Beveridge (1969). "Structural properties of packed beds - A review." The Canadian Journal of Chemical Engineering 47(2): 130-140.

Hyodo, M., et al. (2017). "Undrained monotonic and cyclic shear response and particle crushing of silica sand at low and high pressures." Canadian Geotechnical Journal 54(2): 207-218.

Ismael, N. F. and H. A. Al‐Sanad (1986). "Uplift Capacity of Bored Piles in Calcareous Soils." Journal of Geotechnical Engineering 112(10): 928-940.

Jin, Y.-F., et al. (2018). "Numerical modeling of pile penetration in silica sands considering the effect of grain breakage." Finite Elements in Analysis and Design 144: 15-29.

Kikumoto, M., et al. (2010). "Particle Crushing and Deformation Behaviour." Soils and Foundations 50(4): 547-563.

Kuhn, H. W. and A. W. Tucker (1951). Nonlinear programming. In Proceedings of 2nd Berkeley Symposium, Berkeley, California, USA, University of California Press.

Kuwajima, K., et al. (2009). "Pile Bearing Capacity Factors and Soil Crushabiity." Journal of Geotechnical and Geoenvironmental Engineering 135(7): 901-913.

Lade, P. V., et al. (1996). "Significance of Particle Crushing in Granular Materials." Journal of Geotechnical Engineering 122(4): 309-316.

Lee, K. L. and I. Farhoomand (1967). "Compressibility And Crushing Of Granular Soil In Anisotropic Triaxial Compression." Canadian Geotechnical Journal 4(1): 68-86.

Matsushima, T., et al. (2008). "Microstructural Quantification of Granular Assembly studied by Micro X-ray CT at SPring-8." Journal of applied mechanics 11: 507-515.

McDowell, G. R., et al. (1996). "The fractal crushing of granular materials." Journal of the Mechanics and Physics of Solids 44(12): 2079-2101.

Meyerhof, G. G. (1963). "Some Recent Research on the Bearing Capacity of Foundations." Canadian Geotechnical Journal 1(1): 16-26.

Muir Wood, D. (2007). "The magic of sands— The 20th Bjerrum Lecture presented in Oslo, 25 November 2005This paper represents the written version of the 20th Bjerrum Lecture. While it has been edited for the present publication, it retains the general structure of the original lecture, which was intended for a general geotechnical audience. It deliberately points out some of the still-open questions concerning soil modelling. The Bjerrum Lecture is presented in Oslo in alternate years by the Norwegian Geotechnical Society with the support of the Bjerrum Memorial Fund (Laurits Bjerrums Minnefond)." Canadian Geotechnical Journal 44(11): 1329-1350.

Muir Wood, D. and K. Maeda (2007). "Changing grading of soil: effect on critical states." Acta Geotechnica 3(1): 3-14.

Murff, J. D. (1987). "Pile Capacity in Calcareous Sands: State if the Art." Journal of Geotechnical Engineering 113(5): 490-507.

Nakata, Y., et al. (2001). "Microscopic Particle Crushing of Sand Subjected to High Pressure One-Dimensional Compression." Soils and Foundations 41(1): 69-82.

Oda, M. (1977). "Co-Ordination Number and its Relation to Shear Strength of Granular Material." Soils and Foundations 17(2): 29-42.

Patankar, A. N. and G. Mandal (2014). "The Packing of Solid Particles: A Review." Transactions of the Indian Ceramic Society 39(4): 109-119.

Poulos, H. G. and E. W. Chua (1985). Bearing capacity of foundations on calcareous sand. International Conference on Soil Mechanics and Foundation Engineering, 11th, 1985, San Francisco, USA (Volume 3).

Prandtl, L. (1921). "Hauptaufsätze: Über die Eindringungsfestigkeit (Härte) plastischer Baustoffe und die Festigkeit von Schneiden." ZAMM - Journal of Applied Mathematics and Mechanics / Zeitschrift für Angewandte Mathematik und Mechanik 1(1): 15-20.

Riks, E. (1979). "An incremental approach to the solution of snapping and buckling problems." International Journal of Solids and Structures 15(7): 529-551.

Sadrekarimi, A. and S. M. Olson (2010). "Particle damage observed in ring shear tests on sands." Canadian Geotechnical Journal 47(5): 497-515.

Salgado, R., et al. (2004). "Two- and three-dimensional bearing capacity of foundations in clay." Géotechnique 54(5): 297-306.

Senders, M., et al. (2013). "Piled foundations on the north west shelf." 48: 149-160.

Shahnazari, H. and R. Rezvani (2013). "Effective parameters for the particle breakage of calcareous sands: An experimental study." Engineering Geology 159: 98-105.

Shahnazari, H. and R. J. E. g. Rezvani (2013). "Effective parameters for the particle breakage of calcareous sands: An experimental study." 159: 98-105.

Tengattini, A., et al. (2016). "A constitutive modelling framework predicting critical state in sand undergoing crushing and dilation." Géotechnique 66(9): 695-710.

Thornton, C. (2000). "Numerical simulations of deviatoric shear deformation of granular media." Géotechnique 50(1): 43-53.

Valdes, R. (2003). Fines migration and formation damage: Microscale studies. Ph.D. Dissertation, Georgia Institute of Technology.

Van Langen, H. and P. A. Vermeer (1990). "Automatic step size correction for non-associated plasticity problems." International Journal for Numerical Methods in Engineering 29(3): 579-598.

Van Langen, H. and P. A. Vermeer (1991). "Interface elements for singular plasticity points." International Journal for Numerical and Analytical Methods in Geomechanics 15(5): 301-315.

Vermeer, P. A. and H. Langen (1989). "Soil collapse computations with finite elements." Ingenieur-Archiv 59(3): 221-236.

White, D., et al. (2013). "Geotechnics offshore Australia-beyond traditional soil mechanics." Australian Geomechanics Journal 48(4): 25-47.

Yasufuku, N. and A. F. L. Hyde (1995). "Pile end-bearing capacity in crushable sands." Géotechnique 45(4): 663-676.

Zhang, C., et al. (2013). "The end-bearing capacity of piles penetrating into crushable soils." Géotechnique 63(5): 341-354.

APPENDIX

A. Validation of FEM model

A1. Validation ultimate bearing capacity for shallow foundation by FEM model

Shallow foundation bearing capacity was well solved by classical theory with assumption of rigid plastic failure mechanics. In order to prove the reliability of any FEM model, the validation of the simulations with the classical bearing capacity solution is necessary. Thus, in this study, the validation is performed between the Plaxis with Morh-Coloumb model and the classical bearing capacity for shallow foundation.

A1.1 Theory

Classical bearing capacity solution for shallow foundation was derived analytically by assuming weightless soil ($\gamma'=0$) by Prandtl (1921). In this function, the bearing capacity, q_p, can be expressed in term of cohesion, c, overburden pressure, q_0 and the bearing capacity factors of N_q and N_c.

$$q_p = cN_c + q_o N_q \tag{A-1}$$

$$\text{Where } N_q = \tan^2\left(\frac{\pi}{4} + \frac{\phi'}{2}\right)\exp(\pi \tan\phi') \tag{A-2}$$

$$N_c = (N_q - 1)\cot\phi' \tag{A-3}$$

A1.1 Geometry

A plane strain model with geometry and mesh is shown in Fig. B-1. The foundation width is 2m with the prescribed displacement (of 10% foundation width) is assigned at the top. The model with the width and the length are 7.0m and 5.0m, respectively. The meshing model with 2699 elements of 15-node triangular are generated automatically by Plaxis. Simulations are performed with 5 cases with varying the internal friction from 0.0 to 40.0 degree.

Validation performed in Plaxis with the Morh-Coloumb model (one of available models in Plaxis library). Morh-coloumb is one of the simple models with linear elastic and linear plastic assumptions which are suitable for this validation. By simplify assuming associated flow rule, The

dilation angle is equal to the friction angle ($\psi' = \phi'$) and then the soil's parameter is shortern with only four parameters . The soil's parameters for this validation are given in the table B-1 with the internal friction varies from 0.0 to 40 degree. The cohesion is kept constant with 10.0 kPa.

Table A- 1: Materials parameters for soil with Morh-Coloumb model

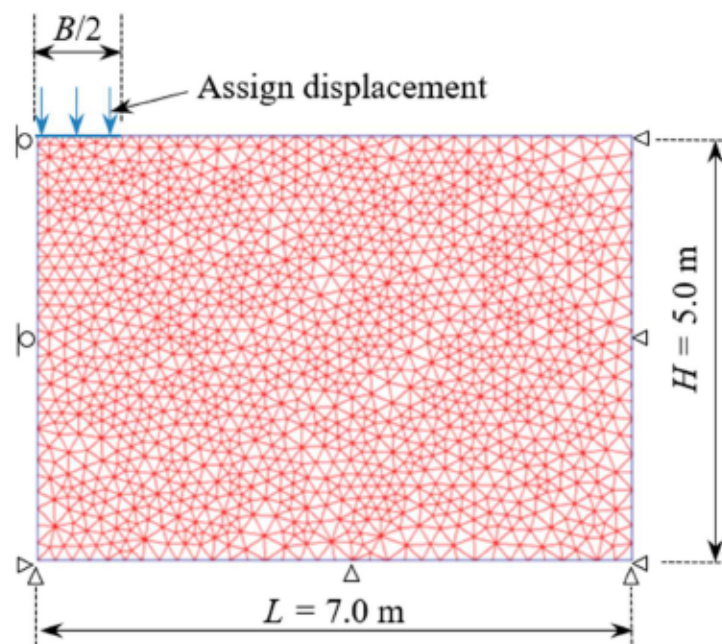| Parameter	Description	Value		Unit
E	Young's Modulus	50,000		(kPa)
v_e	Poisson's ratio	0.35		
ϕ'	internal friction	0.0; 10.0; 20.0;	30.0; 40.0	
c'	cohesion	10.0		(kPa)

Figure A-1: Geometry for shallow foundation
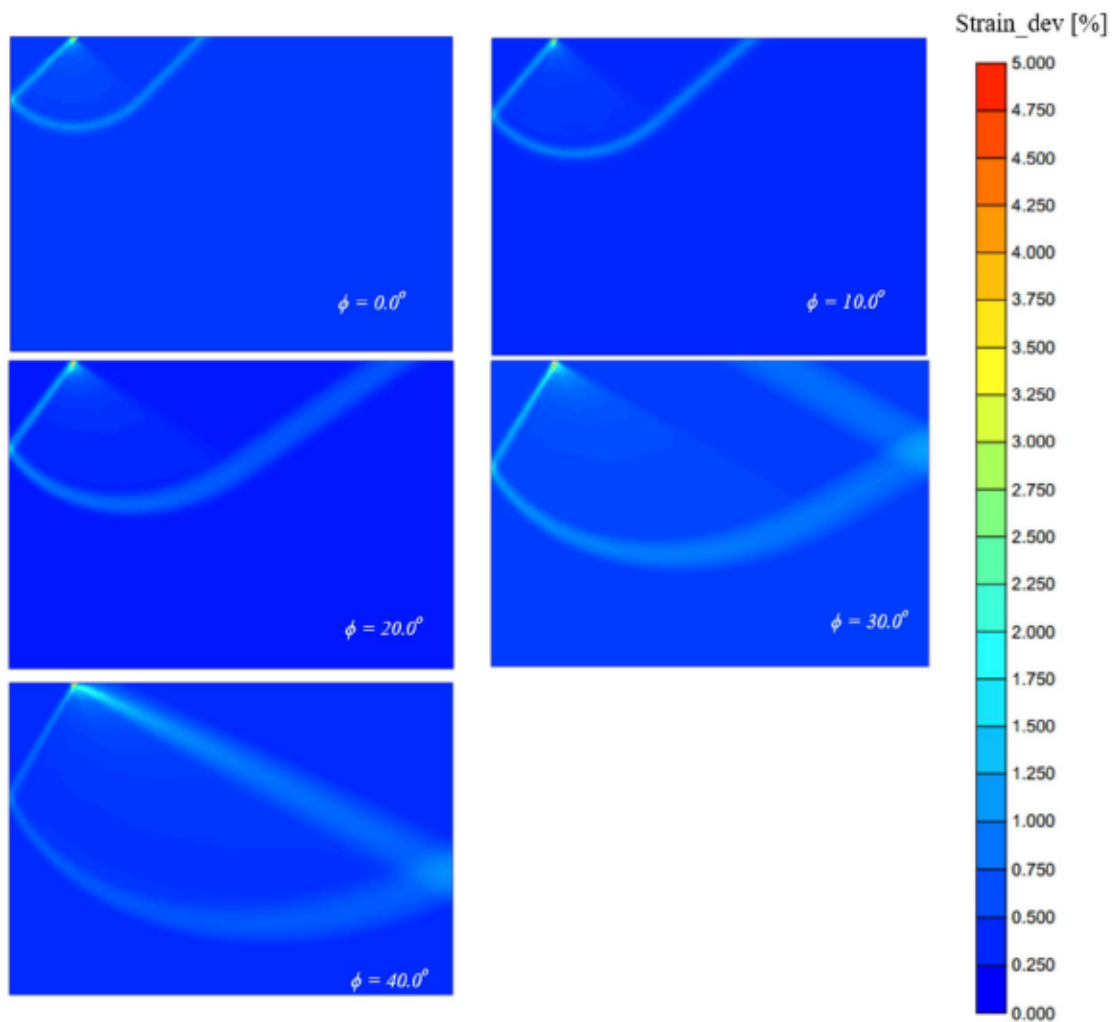
A1.2 Analysis results

Figure A-2: Comparisons of deviator strains in five simulation's cases

The results of different deviator strains in five simulation cases are shown in Fig. A-2. As can be observed from Fig. A-2. The wedge shape created by the distribution of deviator strain below foundation varies with the increase of internal friction angle. The angle $\left(\alpha = \dfrac{\pi}{2} + \dfrac{\phi'}{2}\right)$ derived from analytical method is well matched with the numerical simulations by Plaxis. Moreover, the load-settlement curves by the simulations are agreement with the analytical results by the solution of Prandtl (1921) given in Fig. A-3.
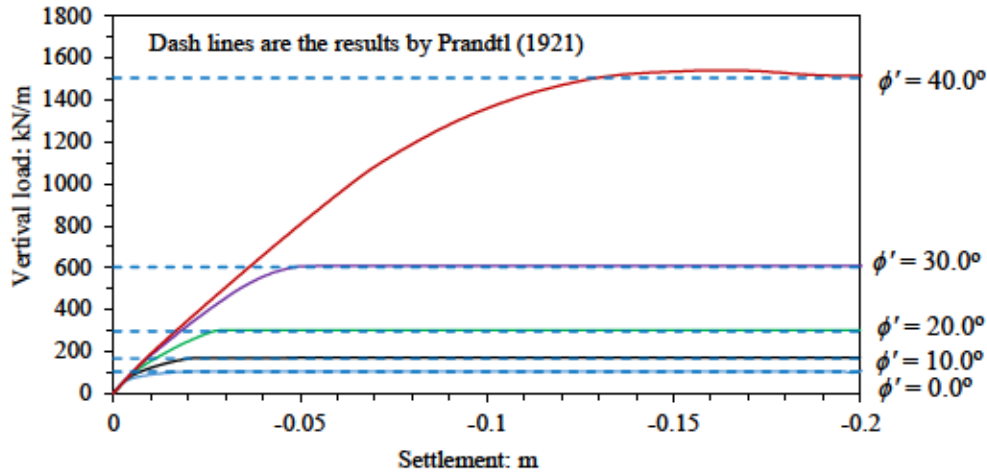
Figure A-3: Comparisons of load- settlement curves of the simulations and the analytical results by Prandtl (1921)

A2. Validation ultimate bearing capacity for circular pile foundation by FEM model

In order to examine the numerical simulation for pile foundation, the validation is also needed. However, there were no exact solution for the problem of bearing capacity of pile foundation. Thus, this section compares the simulation with several approaches.

A2.1 Theory

As mentioned above, there are no exact solution for the bearing capacity problems of pile foundation. Thus, the empirical solution and solution based on finite element analysis are chosen for the validation. For simplicity, the weightless soil is assumed ($\gamma'=0$) and the internal friction is zero ($\phi'=0$). The empirical solution for pile foundation proposed by Meyerhof (1963) is expressed through the shape factor , s_c , and depth factor , d_c , as:

$$q_p = s_c d_c c N_c \leq 9c \tag{A-4}$$

Where $s_c = 1 + 0.2 B_c / L_c$ (A-5)

$d_c = 1 + 0.2 D / B_c$ (A-6)

D is the depth of pile, B_c is pile width, L_c is pile length, $N_c = \pi + 2$ Prandtl (1921)

Another solution based on the rigorously finite element limit analysis by Salgado, Lyamin et al. (2004) . In this study, Salgado, Lyamin et al. (2004), found that the Meyerhof's equation is conservative and may reach to 20-30% .

A2.1 Geometry

Displacement = 0.1D

$L = (0-5)D$

$D/2$

$H = 15m$

$M = 20m$

Pile (D = 2m)
(linear elastic model)
$\upsilon = 0.2;$
$E = 200$ GPa.

Interface element
(smooth or no friction)

Soil
(Morh-Coloumb model)
Cohesive and weightless
$c' = 10.0$ kPa ;
$\upsilon = 0.35;$
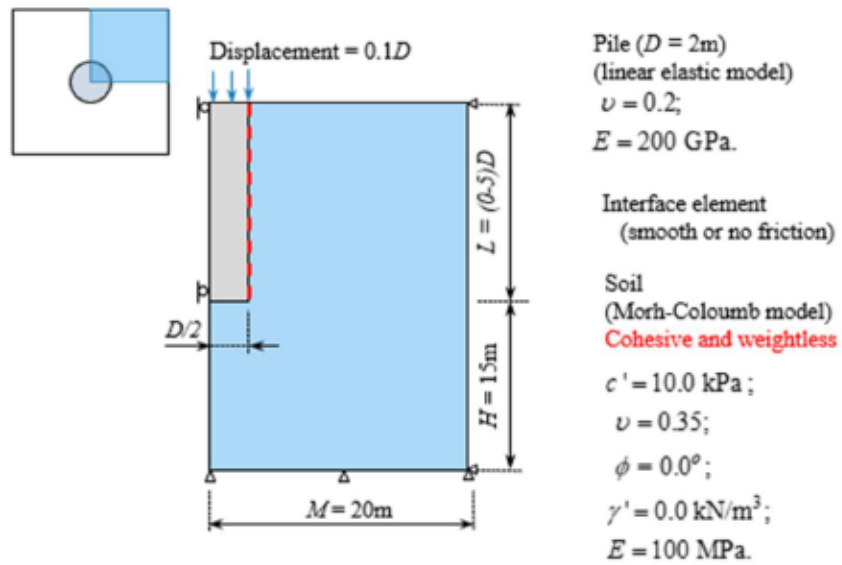$\phi = 0.0°;$
$\gamma' = 0.0$ kN/m³;
$E = 100$ MPa.
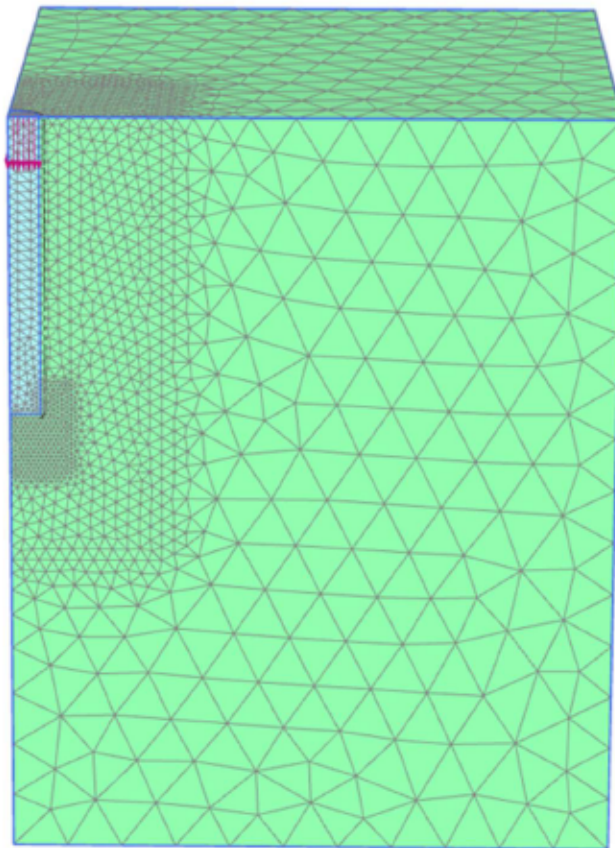
Figure A-4: Geometry for pile foundation

Figure A-5: Meshing model for pile foundation

In order to save calculation time, a quarter of the calculation section was chosen (Fig.A-4). The soil thickness below the pile is 15m, the pile diameter is D = 2m, the pile depth varied from 0B to 5B, and the calculation domain have length 20m. Boundary condition is given as Fig.A-4. The mesh model was generated with 48975 elements 10-node tetrahedral (Fig. A-5). The region around the pile's tip and pile's shaft were carefully meshed while the region outer boundary was defined with coarser mesh. The pile's tip was meshed intensively due to high concentrated stress. Displacement was defined at the pile's head with a value of 10%B. To transfer the surface displacement to the pile's tip is assumed to be very stiff material. Thus, the Young's modulus of pile is assumed to be 200 GPa and linear elastic model is assigned for pile. The pile's material is given in table A-2. While soil's parameter is given in table A-3 with Morh-Coloumb model. Soil is assumed to be cohesive soil with cohesion is 10.0 kPa. The interface element is defined at the interface layer between soil and pile. For this validation, the interface layer plays a role reduces the skin friction to near zero value. Thus, the pile is freely settlement without any skin friction and the pile resistance is only pile' tip bearing.

Table A- 2: Pile parameter with linear elastic model

Parameter	Description	Value	Unit
E	Young's Modulus	200	(GPa)
v_e	Poisson's ratio	0.2	

Table A- 3: Soil's parameter with Morh-Coloumb model

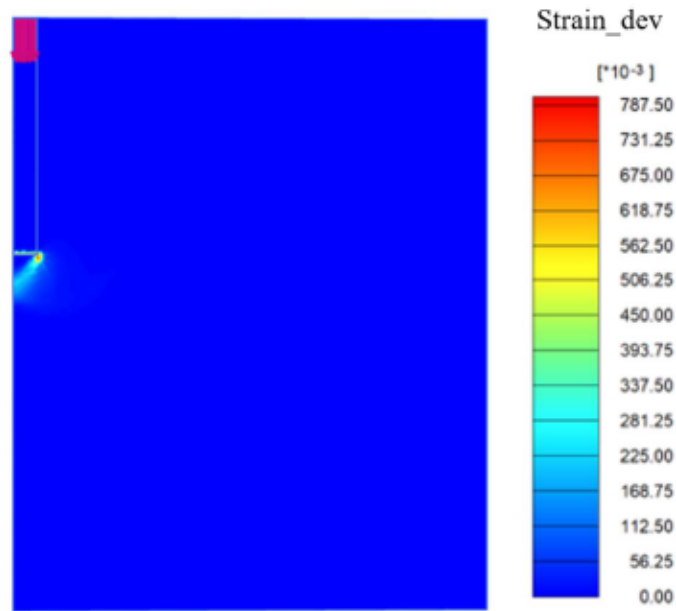| Parameter	Description	Value	Unit
E	Young's Modulus	50,000	(kPa)
v_e	Poisson's ratio	0.35	
ϕ'	internal friction	0.0	degree
c'	cohesion	10.0	(kPa)

A1.2 Analysis results

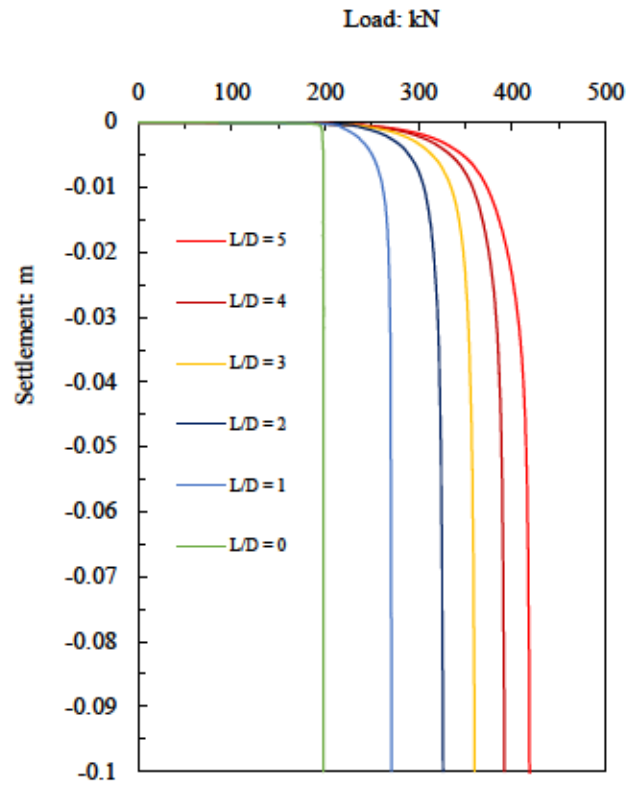*Figure A-6: deviator strain distribution for pile's foundation*

Figure A-7: Load-settlement with different depth ratio

The results of deviator strain distribution is given in the Fig. A-6 with the failure locally at the pile's tip. The failure model may be the punching shear model or local shear model. Next, the load-settlement curves for different depth and pile's diameter ratio L/D is shown in the Fig. A-7. As can be observed from the Fig. A-7, the pile's resistance at the surface $L/D = 0$ has the lowest value. While, when the depth ratio increases the more pile's resistance gain. Finally, comparisons between the empirical solution by Meyerhof (1963), the FEM simulation by Salgado, Lyamin et al. (2004) and the results of simulation are given in the table B-4. The simulation results of bearing capacity factor Nc shows slightly differences from the results of FEM simulation by Salgado, Lyamin et al. (2004). However, the results by Meyerhof (1963) show more conservative especially with the higher depth.

Table A- 4: Comparison the factor N_c by previous approaches and the simulation results

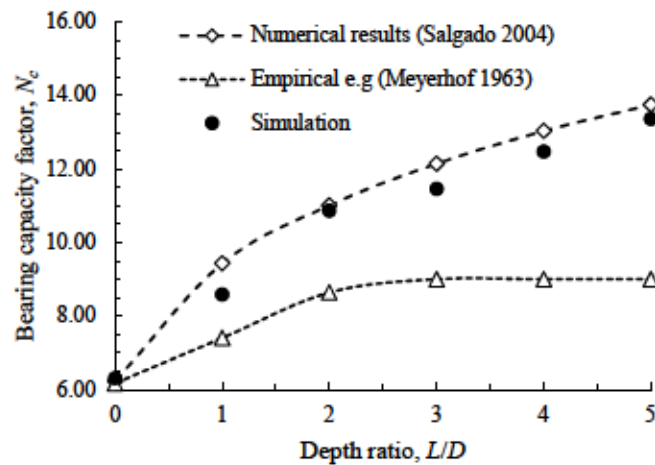| L/D	Bearing capacity factor N_c		
	Salgado (2004)	Meyerhof (1963)	Simulations
0	6.23	6.17	6.30
1	9.43	7.40	8.58
2	11.01	8.64	10.86
3	12.14	9.00	11.45
4	13.03	9.00	12.47
5	13.74	9.00	13.36

Figure A-8: Comparison of the simulation's results, Empirical results by Meyerhof 1963 and Numerical results by Salgado 2004